

## Differential expression of CCR8 in tumors versus normal tissue allows specific depletion of tumor-infiltrating T regulatory cells by GS-1811, a novel Fc-optimized anti-CCR8 antibody

Jessica D. Weaver<sup>a\*</sup>, Edward C. Stack<sup>a\*</sup>, Joshua A. Buggé<sup>a</sup>, Changyun Hu<sup>a</sup>, Lara McGrath<sup>a</sup>, Amy Mueller<sup>a</sup>, Masie Wong<sup>a</sup>, Boris Klebanov<sup>a</sup>, Tanzila Rahman<sup>a</sup>, Rosemary Kaufman<sup>a</sup>, Christine Fregeau<sup>a</sup>, Vikki Spaulding<sup>a</sup>, Michelle Priess<sup>a</sup>, Kristen Legendre<sup>a</sup>, Sarah Jaffe<sup>a</sup>, Dhruvkumar Upadhyay<sup>a</sup>, Anirudh Singh<sup>a</sup>, Chang-Ai Xu<sup>a</sup>, Kristin Krukenberg<sup>a</sup>, Yan Zhang<sup>a</sup>, Yassine Ezzyat<sup>a</sup>, Dorothee Saddier Axe<sup>b</sup>, Michelle R. Kuhne<sup>b</sup>, Michael A. Meehl<sup>a</sup>, Donald R. Shaffer<sup>a</sup>, Brian M. Weist<sup>b</sup>, Dmitri Wiederschain<sup>a</sup>, Fabien Depis<sup>a#</sup>, and Monica Gostissa<sup>a#</sup>

<sup>a</sup>Jounce Therapeutics, Inc., 780 Memorial Drive, Cambridge, MA 02139, USA; <sup>b</sup>Gilead Sciences, Inc., 333 Lakeside Drive, Foster City, CA 94404, USA

### ABSTRACT

The presence of T regulatory (Treg) cells in the tumor microenvironment is associated with poor prognosis and resistance to therapies aimed at reactivating anti-tumor immune responses. Therefore, depletion of tumor-infiltrating Tregs is a potential approach to overcome resistance to immunotherapy. However, identifying Treg-specific targets to drive such selective depletion is challenging. CCR8 has recently emerged as one of these potential targets. Here, we describe GS-1811, a novel therapeutic monoclonal antibody that specifically binds to human CCR8 and is designed to selectively deplete tumor-infiltrating Tregs. We validate previous findings showing restricted expression of CCR8 on tumor Tregs, and precisely quantify CCR8 receptor densities on tumor and normal tissue T cell subsets, demonstrating a window for selective depletion of Tregs in the tumor. Importantly, we show that GS-1811 depleting activity is limited to cells expressing CCR8 at levels comparable to tumor-infiltrating Tregs. Targeting CCR8 in mouse tumor models results in robust anti-tumor efficacy, which is dependent on Treg depleting activity, and synergizes with PD-1 inhibition to promote anti-tumor responses in PD-1 resistant models. Our data support clinical development of GS-1811 to target CCR8 in cancer and drive tumor Treg depletion in order to promote anti-tumor immunity.

### ARTICLE HISTORY

Received 7 June 2022  
Revised 10 October 2022  
Accepted 24 October 2022

### KEYWORDS

CCR8; T regulatory cells; cancer immunotherapy; treg depletion; PD-1 resistance



### Introduction

The immune system has evolved complex cellular and molecular mechanisms to prevent deleterious immune-mediated disorders. A subset of CD4 + T cells, known as T regulatory (Treg) cells, that express the X chromosome-linked transcription factor forkhead box P3 (FOXP3), are central to the prevention of autoimmunity.<sup>1</sup> They act by suppressing aberrant immune responses against self-antigens, resulting in immune tolerance.<sup>2</sup> This tolerance mechanism can be co-opted by tumors when FOXP3+ Tregs, localized to the tumor microenvironment (TME), suppress anti-tumor immunity. Tumor-infiltrating Tregs can disrupt the function of tumor-specific T effector cells through direct cell-cell interactions by engaging inhibitory co-signaling molecules expressed on their cell surface or by secreting anti-inflammatory soluble factors such as transforming growth factor  $\beta$  (TGF $\beta$ ); both mechanisms are known to contribute to the immunosuppressive TME.<sup>3</sup>

The presence of tumor T regulatory cells has been associated with poor prognosis in cancer<sup>4–6</sup> and resistance to immune checkpoint blockade.<sup>7</sup> While immune checkpoint blockade targeting the co-inhibitory molecules cytotoxic


T-lymphocyte-associated protein 4 (CTLA-4) and programmed cell death protein 1/programmed death-ligand 1 (PD-1/L1) has revolutionized the treatment of cancer, the majority of patients do not respond to checkpoint inhibition, and primary and secondary resistance to immune checkpoint blockade is common. Growing evidence suggests that targeting CTLA-4 and PD-1 is insufficient for the full elimination of Tregs within the TME,<sup>8</sup> and PD-1 blockade could even result in enhanced tumor Treg function.<sup>9,10</sup> Thus, new therapies are needed to preferentially deplete Tregs in the tumor while sparing the peripheral pool to ensure continued immune tolerance and minimize immune related toxicities.

A major challenge facing a Treg depletion strategy has been the identification of a specific marker for tumor-infiltrating Tregs. Daclizumab targets the interleukin-2 receptor alpha chain (CD25), which is abundantly expressed on peripheral Treg and T effector cells, leading to broad and relatively non-specific depletion of T cells.<sup>3</sup> Mogamulizumab targets C-C motif chemokine receptor 4 (CCR4), which shows high expression on peripheral Tregs as well as expression on 20–30% of peripheral blood CD4 + T cells.<sup>11</sup> More recently, Plitas

**CONTACT** Monica Gostissa  [mgostissa@jouncetx.com](mailto:mgostissa@jouncetx.com)  Jounce Therapeutics, Inc., 780 Memorial Drive, Cambridge, MA 02139, USA

\*These authors share first authorship

#These authors share senior authorship

 Supplemental data for this article can be accessed online at <https://doi.org/10.1080/2162402X.2022.2141007>

© 2022 Jounce Therapeutics, Inc. Published with license by Taylor & Francis Group, LLC.

This is an Open Access article distributed under the terms of the Creative Commons Attribution-NonCommercial License (<http://creativecommons.org/licenses/by-nc/4.0/>), which permits unrestricted non-commercial use, distribution, and reproduction in any medium, provided the original work is properly cited.

et al. identified C-C motif chemokine receptor 8 (CCR8) as a potential new target on tumor Tregs, reporting that CCR8 was highly expressed on human tumor-infiltrating as compared to peripheral Treg and T effector cells in the TME.<sup>12</sup> Analysis of gene expression data from cancer patient samples also found CCR8 expression to be highly correlated with FOXP3 in Tregs and preferentially expressed on tumor over peripheral Tregs.<sup>13,14</sup>

CCR8 is a cell surface receptor that belongs to class A of the G protein-coupled receptor (GPCR) family. It contains seven transmembrane domains, three extracellular loop domains and three cytoplasmic domains. In addition to tumor Tregs, CCR8 has been reported to also be expressed on T-helper 2 (Th2) cells and innate lymphoid cells,<sup>15</sup> skin-resident memory T cells,<sup>16</sup> monocyte-derived dendritic cells and eosinophils.<sup>17</sup> In the tissues of healthy adults, CCR8-expressing T cells are reported to be unique to skin and not in the small intestine or colon, and only rarely found in peripheral blood.<sup>18</sup> CCR8 has four known ligands of which the best characterized is CCL1, which has been reported to be important for skin homing of T cells, as well as Treg survival and chemotaxis into tumors.<sup>19–21</sup> Thus, the relatively restricted expression pattern of CCR8 and its higher level of expression on tumor-infiltrating Tregs suggests it may be an optimal target for selective depletion of these cells.

Herein, we describe the development and characterization of GS-1811, a humanized monoclonal antibody (mAb) consisting of two identical afucosylated gamma 1 (IgG1) heavy chains and two identical kappa (Igk) light chains, that specifically binds to and inhibits human CCR8 and is designed to selectively deplete tumor resident Treg cells. We show that CCR8 gene expression is restricted to tumor resident Tregs, and that CCR8 protein is expressed at higher densities on tumor resident Tregs than on other tumor resident T cells or circulating peripheral T cells, thus providing a window for tumor-specific Treg depletion. *In vitro*, GS-1811 selectively depletes cells expressing CCR8 receptor at levels observed in human tumor Tregs. Targeting the murine CCR8 receptor results in anti-tumor efficacy *in vivo*, which is dependent on Treg depleting activity, across several tumor models, including tumor types where PD-1 blockade has no effect. Additionally, depletion of the murine CCR8+ tumor resident Tregs induces CD8 infiltration, proinflammatory responses and immunological memory. Finally, anti-CCR8 is a potent combination partner with anti-PD-1 in murine PD-1 resistant models, resulting in improved tumor regression. These data indicate the potential clinical utility of selective depletion of tumor resident T regulatory cells using GS-1811.

## Materials and methods

### PBMCs, tissue samples and cell lines

Human PBMCs were purified from whole blood collected from healthy volunteers (Research Blood Components) by Ficoll-Paque Plus (GE Healthcare) density separation as previously described.<sup>22</sup> Fresh human tumor and normal adjacent tissue (NAT) samples from surgical resections were obtained through the NCI Cooperative Human Tissue Network (CHTN) and the National Research Disease Interchange (NDRI). Human skin

samples from abdominoplasty procedures were provided by BioIVT. All human samples were acquired under approved vendor IRB protocols and were de-identified. The mouse cell line MC38 was kindly provided by Dr. James Allison (MD Anderson Cancer Center) and cultured in DMEM medium (Gibco Life Technologies) supplemented with glutamine and 10% Fetal Bovine Serum (FBS, Sigma). The B16-F10 mouse cell line was obtained from ATCC and cultured in RPMI medium (Gibco Life Technologies) supplemented with glutamine and 10% FBS. The mouse cell lines CT26 and Pan02 were provided by Lab2Pharmacy through ATCC. The mouse MBT-2 cell line was provided by Crown Biosciences. All mouse cells were tested and confirmed negative for Mycoplasma and viral pathogens. For tumor inoculation, cells were expanded for 2 passages after thaw and harvested by trypsin-EDTA treatment when 50–70% confluent. Cells were re-suspended in serum-free, phenol-free DMEM (Thermo Fisher Scientific) and viability >95% was confirmed by trypan blue staining. The human Hut-78 cell line was obtained from ATCC and grown in Xvivo15 medium (Lonza) supplemented with glutamine, 10% human serum, and 1% non-essential amino acids.

### Mice and mouse tumor studies

For all animal studies conducted at Jounce Therapeutics, mice were maintained in accordance with the Jounce Therapeutics Institutional Animal Care and Use Committee (IACUC) protocol JT02-13-19 and were approved by the Jounce IACUC. 6–8 week old female C56BL/6 mice were obtained from the Jackson Laboratories and implanted subcutaneously on the right flank with  $5 \times 10^5$  MC38 cells under isoflurane anesthesia. When tumor volumes reached approximately  $100\text{mm}^3$ , mice were randomized by tumor volume and assigned to treatment groups of 10 (for efficacy studies) or 5 (for immunophenotyping studies) animals per group. Mice were injected intraperitoneally twice weekly for a maximum of three weeks with 200  $\mu\text{g}$  (approximately 10 mg/kg) of anti-mouse CCR8 mIgG2a, anti-mouse CCR8 mIgG1 or isotype control (all from Jounce Therapeutics) prepared in sterile phosphate-buffered saline (PBS). Tumor growth and animal body weights were monitored at least twice weekly. Mice were sacrificed when tumor volumes exceeded  $2000\text{mm}^3$ , tumor became ulcerated, body weight decreased by at least 20% or other signs of clinical distress were noted, in accordance with Jounce protocol JT02-13-19. For the tumor rechallenge study, 10 mice whose MC38 tumors had been previously eradicated by treatment with anti-mouse CCR8 mIgG2a antibody and that had remained tumor free for at least 20 weeks, and 10 age-matched tumor- and treatment-naïve controls were implanted subcutaneously with  $2.5 \times 10^5$  MC38 cells on the left flank and  $1 \times 10^5$  B16-F10 cells on the right flank.

The MBT-2 tumor study was conducted by Crown Biosciences and was approved by their institutional IACUC. During the study, the care and use of animals was conducted in accordance with the regulations of the Association for Assessment and Accreditation of Laboratory Animal Care (AAALAC). 6–8 week old female C3H/He mice were inoculated subcutaneously on the right flank with  $4 \times 10^5$  MBT-2 cells in 100  $\mu\text{L}$  sterile 1x PBS. Mice were randomized into

treatment groups of 10 animals each with an average tumor volume of  $94\text{mm}^3$  and dosed intraperitoneally twice weekly for three weeks with anti-mouse CCR8 mIgG2a (Jounce Therapeutics), InVivoMAb anti-mouse PD-1 RMP1-14 (BioXCell) or mouse IgG2a and rat IgG2a isotype controls (Jounce Therapeutics and BioXCell, respectively). Each antibody was administered at 10 mg/kg, and appropriate isotype controls were added so that the total antibody dose per each group was 20 mg/kg. Mice were checked daily for morbidity and mortality; tumor volume and body weight were measured twice weekly. Mice were sacrificed when tumor volume exceeded  $3000\text{mm}^3$ , tumor ulcerations reached 25% of the tumor surface, body weight loss reached 20% or other signs of clinical distress were noted.

The CT26 tumor study was conducted by Champions Oncology and was approved by their institutional IACUC. Pre-study mice were implanted subcutaneously into the left flank with  $3 \times 10^5$  CT26 cells in 100  $\mu\text{L}$  PBS. Tumor growth was monitored beginning 6–9 days after implantation using digital calipers. Treatment with anti-mouse CCR8 (10 mg/kg) or mouse IgG2a isotype control was started when tumors reached 100 or 250–350 $\text{mm}^3$ . Dosing administration occurred every 3 days for a total of 4 doses. Mice were checked daily for morbidity and mortality; tumor volume and body weight were measured three times weekly. Mice were sacrificed when tumor volume exceeded 1500 $\text{mm}^3$ , tumor ulcerations reached 50% of the tumor surface, body weight loss reached 20% or other signs of clinical distress were noted.

The Pan02 tumor study was conducted by Lab2Pharmacy. All procedures involving the care and use of animals in the study were reviewed and approved by the Stony Brook University Institutional Animal Care and Use Committee (Protocol 748435–3/2015–2182–NF–MI– 5.18.18). Animals were inoculated by subcutaneous injection onto the right dorsal flank while under isoflurane induced anesthesia with  $2 \times 10^6$  cells in 100  $\mu\text{L}$  PBS. Tumor growth was monitored using digital calipers and treatment with anti-mouse CCR8 (10 mg/kg) or mouse IgG2a isotype control was started when tumors reached 100 $\text{mm}^3$ . Dosing administration occurred every 3 days for a total of 4 doses. Mice were checked daily for morbidity and mortality; tumor volume and body weight were measured three times weekly. Mice were sacrificed when tumor volume exceeded 2000 $\text{mm}^3$ , tumor ulcerations reached 25% of the tumor surface, body weight loss reached 20% or other signs of clinical distress were noted.

Treatment windows were chosen based on prior experience with each model, tumor growth kinetics and responsiveness to treatment. For MC38 and MBT-2 models, a standard twice weekly for 3 weeks dosing regimen was used, while for the more responsive CT26 model only 4 doses were administered over 2 weeks. For the Pan02 model, which is known to respond poorly to many IO and non-IO agents,<sup>23</sup> dosing was continued until all mice of the control group reached endpoint.

Tumor volume was calculated using the formula:  $V = (L \times W^2)/2$ , where L is the longest tumor dimension and W is width. Tumor growth and survival curves were obtained using GraphPad Prism. For average tumor growth graphs, the last measurement for mice that reached tumor volume endpoint was carried over until all mice in the same group were

sacrificed. Survival p values were obtained using a pairwise Log-rank (Mantel-Cox) test.

### **Tissue sample dissociation**

Human tumor and NAT samples were processed using the gentleMACS Octo Dissociator (Miltenyi Biotec). Briefly, samples were minced into small fragments in DMEM medium (Gibco Life Technologies) supplemented with 10% FBS (Sigma) on ice, then transferred to a GentleMACS C tube (Miltenyi Biotec) and dissociated using the Miltenyi Tumor Dissociation kit (cat#130-095-929). After a filtration through a 40  $\mu\text{m}$  cell strainer, the cell suspension was centrifuged at 300xg for 5 min, and directly processed for flow cytometry or cryopreserved for later analysis.

Human skin samples (5–50 g, fat layer removed) were minced into approximately 1  $\text{mm}^3$  pieces as above and incubated in PBS + 20 mM EDTA at 37°C for 40 min with constant stirring. The suspension was passed through a 40  $\mu\text{m}$  filter and centrifuged at 300xg for 5 min. Cell pellets were washed once in DMEM+10% FBS and transferred to ice until further processing. For some of the skin samples, the PBS/EDTA step was followed by an enzymatic treatment with 0.5 mg/mL hyaluronidase, 0.1 mg/mL liberase, 6 mg/mL DNaseI and 10 mM HEPES in DMEM for 1 hour at 37°C with constant stirring; this treatment did not increase immune cell yield and did not affect surface marker expression, therefore it was omitted for most of the samples.

Mouse tumor and spleen samples were divided into three sections, and for each tissue one section was processed for IHC (see below), a small piece (approximately 20 mg) was collected in RNAlater (Thermo Fisher Scientific) and processed for RNA extraction (see below). The remaining tissue was collected into 5 mL of DMEM+2% FBS on ice, and mechanically dissociated using a 70  $\mu\text{m}$  cell strainer and the piston of a 5 mL syringe. Dissociated splenocytes were centrifuged at 360xg for 5 min at 4°C, and the cell pellets were resuspended in 1 mL ACK lysing buffer (Gibco) and incubated for 3 min at room temperature (RT) to lyse red blood cells. The reaction was stopped by adding 10 mL DMEM+2.5% FBS, cells were washed twice in 10 mL PBS+2.5% FBS (FACS buffer) and resuspended in FACS buffer for flow cytometry analysis.

### **Flow cytometry**

To prepare human samples for flow cytometry, dissociated cells or PBMCs were washed once in ice cold PBS and stained with the Live/Dead Fixable Near-IR kit (Thermo Fisher Scientific, L34976), following manufacturer's instructions. Cells were then blocked with Human TruStain FcX Block (Biolegend, 422302) and True-Stain Monocyte Blocker (Biolegend, 426102) diluted 1:20 in FACS buffer (PBS + 2% FBS + 0.2 mM EDTA) for 1 hour on ice. After blocking, cells were incubated for 30 min on ice with fluorescently conjugated antibodies to the following surface markers, diluted in Brilliant Stain buffer (BD Biosciences): CD45-BUV396 (BD Biosciences, 563792, 1:100), CD3-FITC (Biolegend, 344804, 1:100), CD4-BUV805 (BD Biosciences, 612887, 1:100), CD14-BV605 (Biolegend, 301834, 1:100), CD56-PerCP/Cy5.5 (Biolegend,

304626, 1:100), CD25-BV711 (BD Biosciences, 563159, 1:20), CCR4-PE (Biolegend, 359412, 1:50), CCR8-BV421 (BD Biosciences, 566379, 1:20) or GS-1811-Dylight 650 (Jounce Therapeutics, 0.8ug/200ul). Samples were then centrifuged at 400xg for 5 min at 4°C and washed once in FACS buffer. After washing, cells were fixed using the FoxP3/Transcription Factor staining kit (Thermo Fisher Scientific) and FoxP3 intracellular staining was performed following manufacturer's instructions for 90 min on ice with anti-human FOXP3-AF647 (Biolegend, 320114,1:20) or -BV421 (Biolegend, 320124, 1:20) antibodies. For quantitative flow cytometry, Quantum Simply Cellular anti-mouse IgG beads (Bangs Laboratories) were stained with anti-CCR8 or anti-CCR4 antibodies diluted in Brilliant Stain buffer for 30 min on ice. Following incubation, cells or beads were washed two times in FACS buffer and acquired on a BD LSRFortessa flow cytometer. Data were analyzed with FlowJo. Live CD45+ events were identified, then CCR8 or CCR4 expression was assessed in immune cell subsets. Tregs were identified as CD3+ CD4+ FoxP3+, while non-Treg CD3+ CD4+ FoxP3- cells were defined as Tconv. CD8 T cells were identified as CD3+ CD4-. Fluorescence-minus-one (FMO) and isotype controls were used to define positive and negative populations. Percentage of CCR8 or CCR4 positive events, and median fluorescence intensity (MedFI) of positive populations were established for each cell subset. MedFI values were used to calculate CCR8 and CCR4 median copies per cell values using standard curves of quantification beads and the manufacturer's provided excel sheet. Values were only reported if more than 50 cells from any specific immune cell subset could be clearly enumerated. Statistical comparisons between populations were calculated with unpaired two-tailed t tests using GraphPad Prism software.

A similar procedure was used for mouse samples flow cytometry. Samples were stained with eFluor780 fixable viability dye (Thermo Fisher Scientific, 65-0865-14) at 1:2,000 dilution in 1x PBS at RT for 10 min, then incubated with a cocktail of antibodies to extracellular markers prepared in FACS buffer containing 1:50 TruStain FcX Fc block (Biolegend, 101319). The following anti-mouse Abs were used: CD45-BV510 (Biolegend,103138, 1:150), CD3-BUV395 (BD Biosciences, 563565, 1:50), CD4-BUV737 (BD Biosciences, 564298, 1:100), CD8-PerCP/Cy5.5 (Biolegend, 100734, 1:100), CD19-BV785 (Biolegend,115543, 1:50), CD25-AF488 (Thermo Fisher Scientific, 53-0251-82, 1:100), PD-1-PE (Biolegend,109104, 1:100), CCR8-BV421 (Biolegend, 150305, 1:100), F4/80-BV605 (Biolegend,123133, 1:100), and CD11b-BV711 (Biolegend,101242, 1:100). After washing, fixation and permeabilization as above, cells were incubated with FoxP3-AF700 antibody (Thermo Fisher Scientific, 56-5773-82, 1:50) in 1x permeabilization buffer (Thermo Fisher Scientific) on ice for 90 min, washed and acquired on a BD LSRFortessa flow cytometer. Data were analyzed with FlowJo and GraphPad Prism software. Tregs were identified as CD3+ CD4+ CD25+ FoxP3+, while CD3+ CD4+ CD25- FoxP3- non-Treg cells were defined as Tconv.

### **Immunohistochemistry and image analysis**

Commercially sourced human skin samples were fixed for 24 hours in 10% neutral buffered formalin, then processed on

the Leica ASP300S Tissue Processor through a graded series of alcohols (70% > 80% > 95% > 100%) prior to xylene, and then ASP Parablock paraffin wax. Once the tissue was processed, it was embedded in Paraplast Plus paraffin into a block, which was then sectioned at 5um onto glass slides to be used for IHC staining. FoxP3 (Abcam, clone 236A/E7) and CD8 (Dako, clone C8/144B) staining was performed on a Bond RX. Antigen retrieval, peroxide block, and washes preceded primary antibody incubation (FoxP3 or CD8, 1:100). Slides were again washed prior to secondary antibody application and subsequent Refine Red chromogen (Leica). Slides were finally incubated in Hematoxylin prior to coverslipping. After staining, each skin tissue sample was scanned into Halo. Annotation areas were created so that analyses of FoxP3 and CD8 IHC would take into account the epidermal and dermal layers. Once tissue annotations were complete, the Indica Labs - Cytonuclear v 1.6 module was used to create specific algorithms for the detection of FoxP3+ and CD8+ cells in all epidermal and dermal layers. Once image analysis was completed, all data were exported into .csv and various sample metrics were evaluated for percent positivity and density assessments.

Samples from mouse tumor studies were embedded and sectioned as above, then stained for FoxP3 (CST, clone D608R) and CD8 (Abcam, clone EPR20305) at 1:100. Staining was performed on a Bond RX. Antigen retrieval, peroxide block, and washes preceded primary antibody incubation (FoxP3 or CD8, 1:100). Slides were again washed prior to secondary antibody application and subsequent DAB chromogen (BOND polymer Refine Detection System). Slides were then incubated in Hematoxylin prior to coverslipping. Once stained, the slides were scanned into Halo and manual digital annotations were created to identify tumor regions where analyses were to be focused. For quantification, we set about to segment every cell within the analysis of tumor regions using both the signal from the IHC, as well as from the hematoxylin counterstain present in each image. This allowed for the identification of either CD8+ or FoxP3+ cells. Once image analysis was completed, all data were exported into .csv and analyses were performed using both Excel and Prism. ANOVA was used to compare the three treatment arms, while unpaired post-hoc t-tests, when appropriate, were used to evaluate differences between the individual treatment arms.

### **NanoString gene expression analysis of MC38 tumor samples**

Samples from MC38 tumors were collected at day 3 after a single Ab dose (anti-mouse CCR8 mIgG2a, anti-mouse CCR8 mIgG1 and isotype control, n = 4 each) and stored in RNAlater (Invitrogen). RNA was extracted and quantified using the Maxwell SimplyRNA Tissue kit (Promega) and the Quantifluor RNA High Standard kit (Promega). Residual genomic DNA was removed using the Turbo DNA-free kit (Invitrogen). Gene expression was measured with the NanoString platform using the nCounter Mouse Immunology Panel. Quality control was conducted on field of view, binding density, positive and negative control probes, and estimated RNA amount. Raw gene expression values from RCC files were

normalized to housekeeping genes, log<sub>2</sub> transformed, and floored to the 95<sup>th</sup> percentile of negative control genes. Differential gene expression analysis was conducted for comparison across treatment groups using unpaired t-tests, with false discovery rate (Benjamini-Hochberg procedure) p-value correction. Gene set enrichment analysis (GSEA) was performed using the Hallmark gene sets from the MSigDB collections.<sup>24,25</sup>

### Identification of Treg-specific targets using bioinformatics screen

To identify a list of potential targetable Treg-specific genes, a bioinformatics screen was conducted using gene expression profiles of human cancer patient tumors and peripheral blood of healthy donors. First, a list of genes was identified as correlated with a Jounce-generated Treg gene signature across RNA-seq profiles of human tumor samples in TCGA. This list was further pruned to targets amenable to an antibody therapeutic modality with predicted cellular membrane bound or secreted localizations, and targets with preferential expression in tumor-infiltrating Tregs relative to tumor-infiltrating conventional T cells and other peripheral blood cell types. Additional functional qualifications were utilized to derive a list of 32 Treg genes and further select CCR8 as preferred target for therapeutic antibody discovery.

### Analysis of CCR8 and Treg markers gene expression in human datasets

To analyze Treg markers gene expression, processed single-cell RNA-seq datasets from samples from melanoma, head and neck cancer, and hepatocellular carcinoma patients were downloaded from Gene Expression Omnibus, accession numbers: GSE72056, GSE103322, GSE98638.<sup>26–28</sup> All files were processed in R using Seurat with cells filtered using parameters: min cell per sample = 3, min genes per cell = 200, max mitochondrial genes = 5%. Gene expression measurements were normalized for each cell by total expression, multiplied by scaling factor (10,000 by default) and log transformed. Gene expression measurements were scaled to regress out sources of technical noise or batch effects including batch, cell alignment rate, number of detected molecules (nUMI), mitochondrial gene expression, and cell-cycle, where applicable. For combining datasets, log normalized gene expression values were then normalized against a housekeeping gene set across cells.<sup>29</sup> In post-processing, expression of cell-type markers or signatures (e.g. CD8A for CD8 T cells, FOXP3 for Tregs) were used to identify cell clusters. Gene expression of Treg markers were visualized using FeaturePlot with TSNE as the reduction method.

To analyze CCR8 gene expression in TCGA tumor vs adjacent normal tissues, TCGA RNA-seq gene-level expression data were downloaded from Omicsoft Array Studio from the TCGA\_B37 data pulldown. Gene expression measurements were reported in log<sub>2</sub>(FPKM +0.01). All samples from primary tumors and adjacent normal tissues in solid tumor types are considered. Differential expression analysis between CCR8 levels in tumor samples compared to adjacent normal samples

within each tumor type was conducted using unpaired, one-tailed Mann-Whitney U test.

### Generation and humanization of GS-1811

The parent antibody of GS-1811 was selected using mouse hybridoma technology from animals immunized with CCR8 + cells or with human CCR8 expression plasmid DNA. Resulting clones were identified that demonstrated robust binding to CHO cell lines overexpressing human CCR8 but lacked binding to parental CHO cells or CHO cells expressing the CCR4 family member. Paired mouse VH and VL IgG DNA sequences were obtained from lead hybridomas for production. Chimeric versions of parental antibodies were generated by grafting mouse VH/VL regions onto human IgG1/kappa isotype backbone. Lead chimeras that specifically bound to CHO-CCR8 cells were humanized according to standard techniques. Briefly, the six complementarity determining regions (CDRs) were identified and grafted onto human IGHV/IGKV germline frameworks identified via sequence and structural homology. Back mutations to the mouse germline were selected to maintain residues at the VH/VL interface and in the canonical loop structure. Humanized Fv sequences were cloned with human IgG1/kappa constant domains to produce a panel of humanized antibodies. GS-1811 was selected from this panel based on affinity and biophysical characteristics. Since a reduction in core fucosylation on amino acid N297 in the CH2 domain of the IgG1 Fc region has been shown to enhance ADCC function of antibody via improved CD16a binding,<sup>30</sup> GS-1811 was expressed in FUT8<sup>-/-</sup>-CHO-GS cell line at Jounce and shown to be completely afucosylated as compared to an intact Ab standard (Waters Corp) by glycan analysis performed on UPLC with Glycan BEH Amide column following PNGase F enzyme treatment.

### On-cell affinity assessment of GS-1811

To assess specific binding to GS-1811 to hCCR8, CHO-S cell lines overexpressing hCCR8, hCCR4 or parental CHO-S were plated at  $1 \times 10^5$  cells/well in a 96-well plate and incubated with increasing concentrations (10-point 4-fold titration starting at 100 µg/ml) of GS-1811 or isotype control for 30 min at 4°C. After two washes in FACS buffer, cells were incubated for additional 30 min at 4°C with an anti-human IgG-AF647 secondary antibody (Biolegend, 409320, 1:100), washed twice in FACS buffer and acquired on a BD LSRFortessa flow cytometer. Each condition was run in triplicates. Data were analyzed with FlowJo and GraphPad Prism software.

The monovalent equilibrium dissociation constant ( $K_D$ ) of purified GS-1811 antibody molecules to CHO-S cells expressing human CCR8 was determined using a solution equilibrium titration (SET) assay. Briefly, fixed concentrations (0.2, 0.1 and 0.05 nM) of GS-1811 were incubated for 3 hours at 37°C with increasing concentrations (11-point two-fold titration starting at  $1.5 \times 10^7$  cells/mL) of CHO-S cells expressing ~300,000 copies of human CCR8 per cell. After equilibrium was reached, the samples were centrifuged at 500xg for 5 min and the supernatant, containing unbound antibody, was quantified on the Meso Scale Discovery (MSD) instrument (MESO

QuickPlex SQ 120) using anti-IgG coated MSD plates and a SULFO-TAG anti-human IgG secondary antibody (MSD). The concentration of unbound antibody as a function of human CCR8-overexpressing CHO cell concentration was plotted using GraphPad Prism software. The signal from the MSD plate and known concentrations of the antibody and cells were then used to calculate the  $K_D$  of the complex using a 1:1 binding model of the bimolecular equilibrium interaction. The fitting was done using a custom-built script on Mathematica software. Three independent replicate plates were tested and  $K_D$  values were averaged together.

### **Assessment of GS-1811 antagonism of CCL1/CCR8 interaction**

The DiscoverX PathHunter  $\beta$ -Arrestin assay (Eurofins) was used to determine GS-1811 antagonist activity. GS-1811 or isotype control were serially diluted starting at 30  $\mu\text{g}/\text{mL}$  to form a 10-point 3-fold dilution curve in assay buffer and added to the PathHunter eXpress  $\beta$ -Arrestin GPCR cells expressing human CCR8. Following a 30 min incubation at 37°C, 5%  $\text{CO}_2$ , human CCL1 (Peprotech) was added at the final concentration of 13.7 nM and incubated for additional 90 min. Signal was generated through a single addition of PathHunter Detection reagent cocktail, followed by a 60 min incubation at room temperature. Chemiluminescent signal generated was measured with the PerkinElmer Envision instrument. Each condition was run in triplicate. Data were analyzed with GraphPad Prism software.

### **ADCC assays**

Human NK cells were isolated from fresh human healthy donor PBMCs by magnetic separation using the EasySep Human NK Cells Isolation Kit (StemCell Technologies) according to the manufacturer's protocol. Alternatively, purified frozen human NK cells were obtained from StemCell Technologies.

To evaluate GS-1811-mediated ADCC, a panel of recombinant CHO-S cell lines was generated expressing a range of CCR8 densities. CHO-S cells expressing either ~10,000, ~5,000, ~2,500, ~1,500, or ~600 copies of human CCR8 per cell, along with parental CHO-S cells, were stained with CellTrace Blue Dye (Thermo Fisher Scientific) according to manufacturing protocol, resuspended in RPMI Medium (Gibco) supplemented with Glutamine and 10% FBS (Sigma) and counted.  $2 \times 10^4$  CHO-S cells were mixed with  $1 \times 10^5$  purified human NK cells in 96-well plates, so that the final effector to target ratio was 5:1. GS-1811, its fucosylated version (either in chimeric or fully humanized formats) and isotype controls were serially diluted to generate a 10-point curve with 10-fold intervals starting at 10  $\mu\text{g}/\text{mL}$ , added to designated wells and the plates were incubated at 37°C overnight. Each condition was run in triplicate for each NK cell donor. The next day, cells were washed in FACS buffer and prepared for flow cytometry. Cells were incubated for 30 min at 4°C with labeled antibodies against CD56 (1:100) to identify NK Cells and eFlour780 Viability dye (1:1000) to identify dead cells. After the incubation, plates were washed 3 times with FACS

buffer and acquired on a BD LSRFortessa flow cytometer. Analysis was performed with FlowJo. Percent of specific lysis was calculated by normalizing values to isotype control at any given antibody concentration. Data were analyzed in GraphPad Prism to determine EC50 values.

ADCC assays with Hut78 cells, endogenously expressing CCR8 densities within the range of expression on tumor-infiltrating Tregs, were conducted as described above, but omitting the CellTrace Blue staining step and with a starting antibody concentration of 1 mg/mL. Three independent NK cell donors were tested, and each condition was run in triplicate. The flow cytometry panel included CD3-AF488 (Biolegend, 300320), CD4-BV421 (Biolegend, 317434), CD56-PE (BD Biosciences, 555516) at 1:100 dilution. Live Hut78 cells were identified from all events by gating on CD4+ and viability dye negative events. Percent killing compared to control was determined following the equation: (Isotype-GS-1811)/Isotype\*100, where "Isotype" is the average of the isotype control triplicates and "GS-1811" is one replicate of the GS-1811 condition. These values were analyzed in GraphPad Prism to determine EC50 values for ADCC potency.

For TIL ADCC assays, three cryopreserved TIL samples were thawed, processed with STEMCELL EasySep Dead cell removal Kit (StemCell Technologies) following manufacturer's instructions and resuspended in 1600  $\mu\text{l}$  RPMI with glutamine and 10% FBS. 100  $\mu\text{l}$  of TIL cell suspension were then incubated as above with  $1 \times 10^5$  purified human NK cells from two independent donors, in the presence of either chimeric GS-1811 or isotype control at 1  $\mu\text{g}/\text{mL}$ . After overnight incubation at 37°C, cells were analyzed by flow cytometry with the following panel: Live/Dead Fixable Near-IR kit (Thermo Fisher Scientific, L34976), CD45-BUV396 (BD Biosciences, 563792), CD3-AF488 (Biolegend, 300320), CD4-BV711 (Biolegend, 317440), CD56-PE (BD Biosciences, 555516), and FOXP3-BV421 (Biolegend, 320124). Treg killing was assessed by comparing the frequency of live FOXP3+ cells within CD4 T cells in GS-1811-treated and control samples. The results were assessed with a two tailed student's T test.

## **Results**

### **CCR8 expression is highly restricted to tumor-infiltrating Tregs**

To identify novel therapeutic targets that could enable specific depletion of tumor-infiltrating Treg cells, we conducted an in-silico screen using The Cancer Genome Atlas (TCGA) followed by a series of custom designed filters. This approach (Figure 1a) led to the identification of 32 genes with preferential expression in tumor-infiltrating Tregs and with putative extracellular domains amenable to antibody targeting. Analysis of publicly available single cell RNA sequence datasets revealed that expression of one of these genes, CCR8, was exquisitely restricted to CD4+ CD25 (IL2RA)+ FoxP3+ cells as opposed to other Treg markers such as CD25 itself, CTLA-4, GITR (TNFRSF18), TIGIT, and CCR4 (Figure 1b and Supplementary Figure 1a). In TCGA, CCR8 gene expression was found to be higher in primary tumors than in normal adjacent tissues across many indications (Figure 1c). We assessed surface expression of CCR8

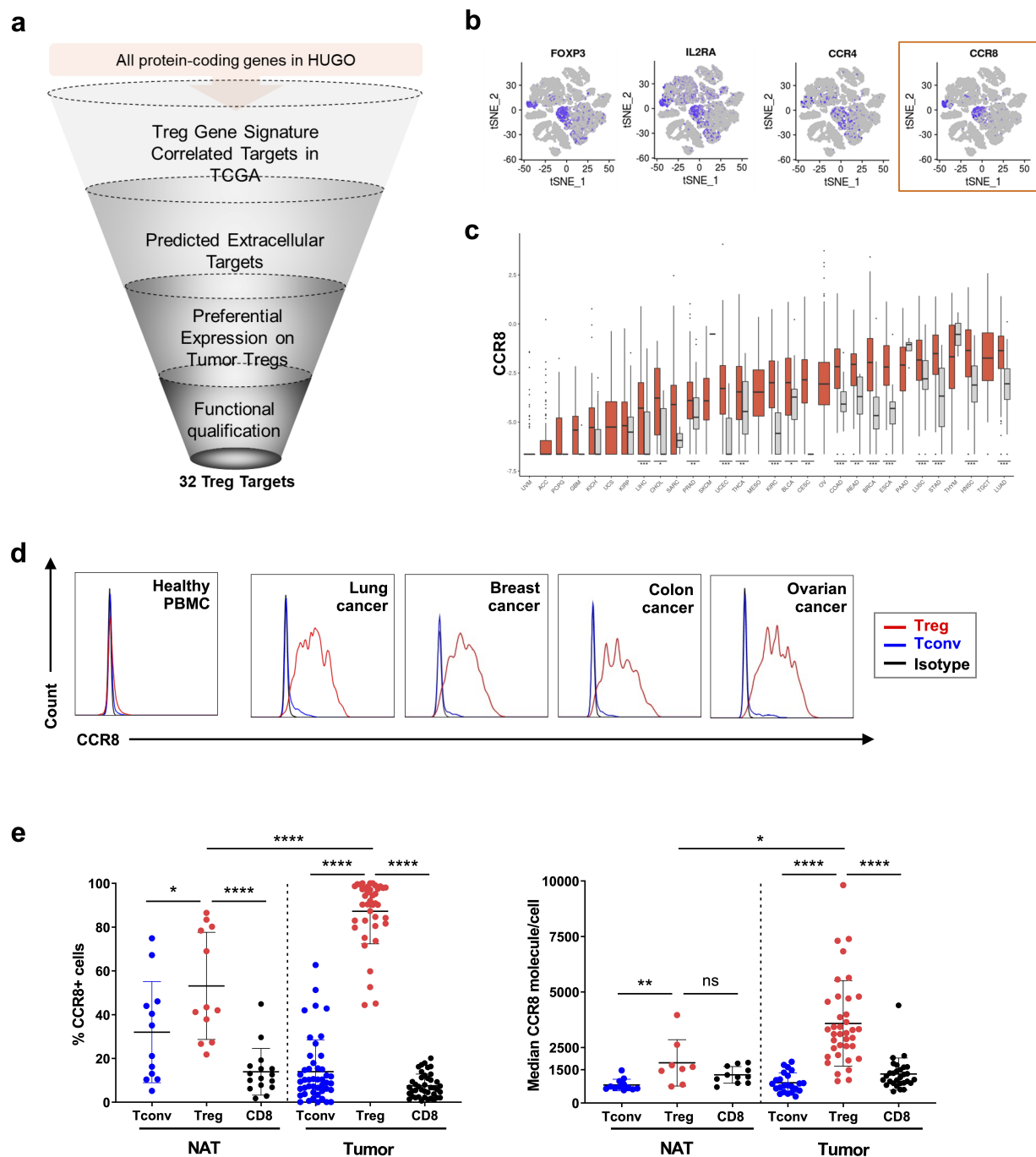


**Figure 1.** CCR8 expression is highly restricted to tumor-infiltrating T regulatory cells in human tumors of different lineage.

a) Schematic of the Treg bioinformatic screen used to identify putative targets for Treg depletion. b) t-SNE plots displaying single cell RNAseq gene expression profiles from 43 patients (HCC n=9, HNSCC n=18, melanoma n=19) including tumors, blood, LN and normal tissue that were combined and characterized by cell marker genes, as indicated. c) Gene expression analysis on bulk RNA-seq (TCGA) from primary tumor samples (red bars) and adjacent normal tissues (gray bars). The degree of statistical significance between tumor and adjacent normal samples is indicated below each pair of boxplots with tumor types (\*\*\*\*:  $p < 0.0001$ ; \*\*\*:  $p < 0.01$ ; \*\*:  $p < 0.05$  from unpaired, one-tailed Mann-Whitney U tests). d) Flow cytometry analysis of peripheral blood mononuclear cells (PBMC) from healthy donors and indicated freshly dissociated human tumor samples. FoxP3 staining was used to identify T cell populations within CD45/CD3/CD4+ cells, and CCR8 expression was evaluated in Treg (FoxP3+, red histograms) and non-Treg (Tconv, FoxP3-, blue histograms) cells. Isotype control histograms are shown in black for total CD3+ T cells. Healthy PBMC data is representative of 3 independent donors. e) Percentage of CCR8+ cells (left) and median density of CCR8 molecules per cell (right) in Tconv (blue), Treg (red) and CD8 T cells (black) in freshly dissociated human tumor samples (Tumor) or normal adjacent tissue (NAT). Indications include breast, head and neck, lung, ovarian, colon, and bladder cancer. T cell populations were identified as in (d). Each data point represents a single sample. Error bars represent standard deviation from the average. The degree of statistical significance between populations indicated on top of the graphs (\*\*\*\*:  $p < 0.0001$ ; \*\*\*:  $p < 0.01$ ; \*\*:  $p < 0.05$ ; ns: no significant difference).

by flow cytometry and found preferential expression of CCR8 on tumor Tregs as compared to both peripheral Tregs and tumor and peripheral non-Treg CD4+ cells (referred to as T conventional cells, Tconv) (Figure 1d). We then expanded this analysis by comparing matched tumor and normal adjacent

tissue samples from multiple indications, confirming highest CCR8 expression in tumor Tregs. Importantly, precise quantitative flow cytometry analysis showed that tumor CCR8+ Tregs express a significantly higher number of CCR8 molecules on a per-cell basis than any other T cell subsets, including CD8

T cells (Figure 1e). On the contrary, we found CCR4 to be broadly expressed on tumor and peripheral T cell subsets (Supplementary Figure 1b). As CCR8 has been identified as a marker of tissue-resident T cells in the skin,<sup>16,31</sup> we assessed its expression in skin samples, and compared it to CCR4 expression. Both CCR8 and CCR4 were expressed on all skin T cell subsets, at relatively high levels as compared to peripheral blood and other normal tissues (Supplementary Figure 2a). However, absolute numbers of T cells in the skin were low, with Tregs and CD8 T cells accounting for only 0.4% and 0.6% of total cells respectively, as determined by IHC analysis (Supplementary Figure 2b). The relatively restricted expression pattern of CCR8 and its higher level of expression on tumor-infiltrating Tregs suggests it may be a good target for selective depletion of these cells.

### Treatment with an anti-mouse CCR8 antibody results in robust antitumor efficacy in mouse models and synergizes with PD-1 blockade

CCR8 is conserved in mouse and its expression is restricted to mouse tumor-infiltrating Tregs (Supplementary Figure 3). We therefore sought to investigate the therapeutic effect of treatment with an anti-mouse CCR8 antibody (Ab) in a series of

syngeneic mouse tumor models. In the MC38 model, administration of anti-mouse CCR8 Ab (murine IgG2a, mIgG2a) resulted in significant tumor growth inhibition with about 30–50% of mice showing complete tumor regression (Figure 2a and Figure 3a). Robust efficacy was also observed in the Pan02 tumor model (Figure 2b), which is reported to be poorly responsive to immuno-oncology therapeutics<sup>23</sup> and in the CT26 tumor model, where efficacy was maintained even when treatment was started following establishment of large tumors (Figure 2c). Lastly, we assessed the impact of anti-CCR8 mIgG2a treatment in combination with anti-PD-1 in the PD-1-resistant model MBT-2. Anti-mouse CCR8 mIgG2a monotherapy inhibited tumor growth compared to isotype control, while anti-PD-1 monotherapy did not. The combination of anti-mouse CCR8 mIgG2a and anti-PD-1 resulted in increased efficacy compared to anti-mouse CCR8 mIgG2a monotherapy with complete tumor regression observed in half of the animals receiving combination therapy compared to no complete responses in animals receiving either monotherapy or isotype control (Figure 2d). Of note, no signs of treatment-related toxicities or body weight loss were observed in any of these studies, even when anti-mouse CCR8 Ab was administered for an extended period of time, such as in the Pan02 study (Supplementary Figure 4).

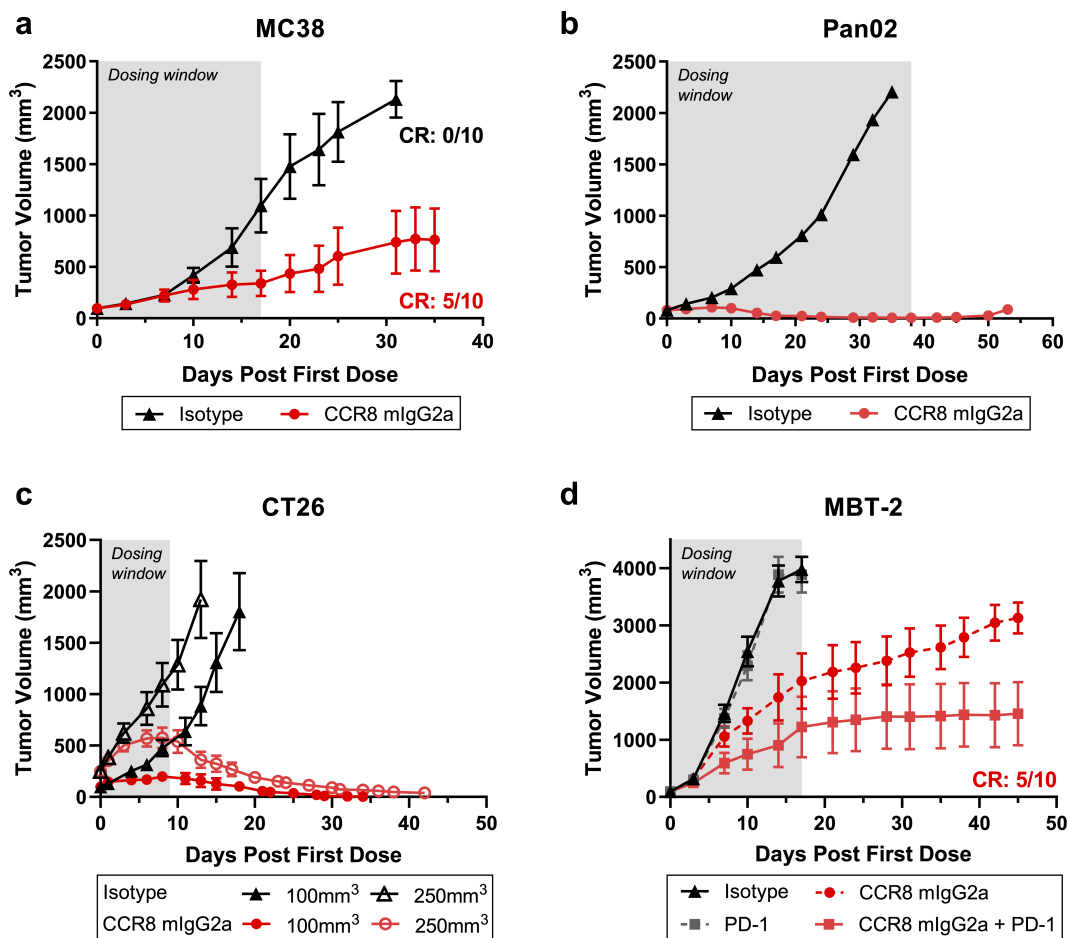


**Figure 2.** Anti-mouse CCR8 antibody treatment results in robust antitumor efficacy in mouse tumor models and synergizes with PD-1 blockade. Tumor growth analysis of cohorts of mice bearing MC38 (a), Pan02 (b), CT26 (c) or MBT-2 (d) tumors and treated with the indicated antibodies. Mice were randomized into treatment groups when average tumor volume was approximately 100mm<sup>3</sup>, except in (b) where average tumor volume at randomization was either 100mm<sup>3</sup> or 250 mm<sup>3</sup>. Day0 indicates day of first dose. Tumor growth curves show average  $\pm$  SEM; CR corresponds to the number of complete responses in each group.



### Depletion of CCR8<sup>+</sup> tumor-infiltrating Tregs is required for antitumor efficacy of anti-mouse CCR8 Ab

To demonstrate that Treg depletion is a major determinant of response to anti-mouse CCR8 Ab treatment, we took advantage of the fact that only antibodies with murine IgG2a and not murine IgG1 Fc regions are able to engage the FcγR and mediate antibody-dependent cellular cytotoxicity (ADCC).<sup>32</sup> We therefore compared the effect of both versions of the anti-mouse CCR8 Ab in the MC38 model. As shown in Figure 3a, only the mIgG2a version inhibited tumor growth, while the

mIgG1 version did not show efficacy as compared to isotype control. We then assessed immune cell composition of MC38 tumors from mice treated with either one or two doses of anti-CCR8 mIgG2a or mIgG1 Abs by flow cytometry. Consistent with the proposed mechanism of action, only the Fc-competent version of the anti-mouse CCR8 Ab (mIgG2a) and not the mIgG1 version resulted in robust Treg depletion in the tumor (Figure 3b, left panel, and Supplementary Figure 5a). This observation was also confirmed by immunohistochemistry (IHC) on the same tumor samples (Figure 3c). Depletion of

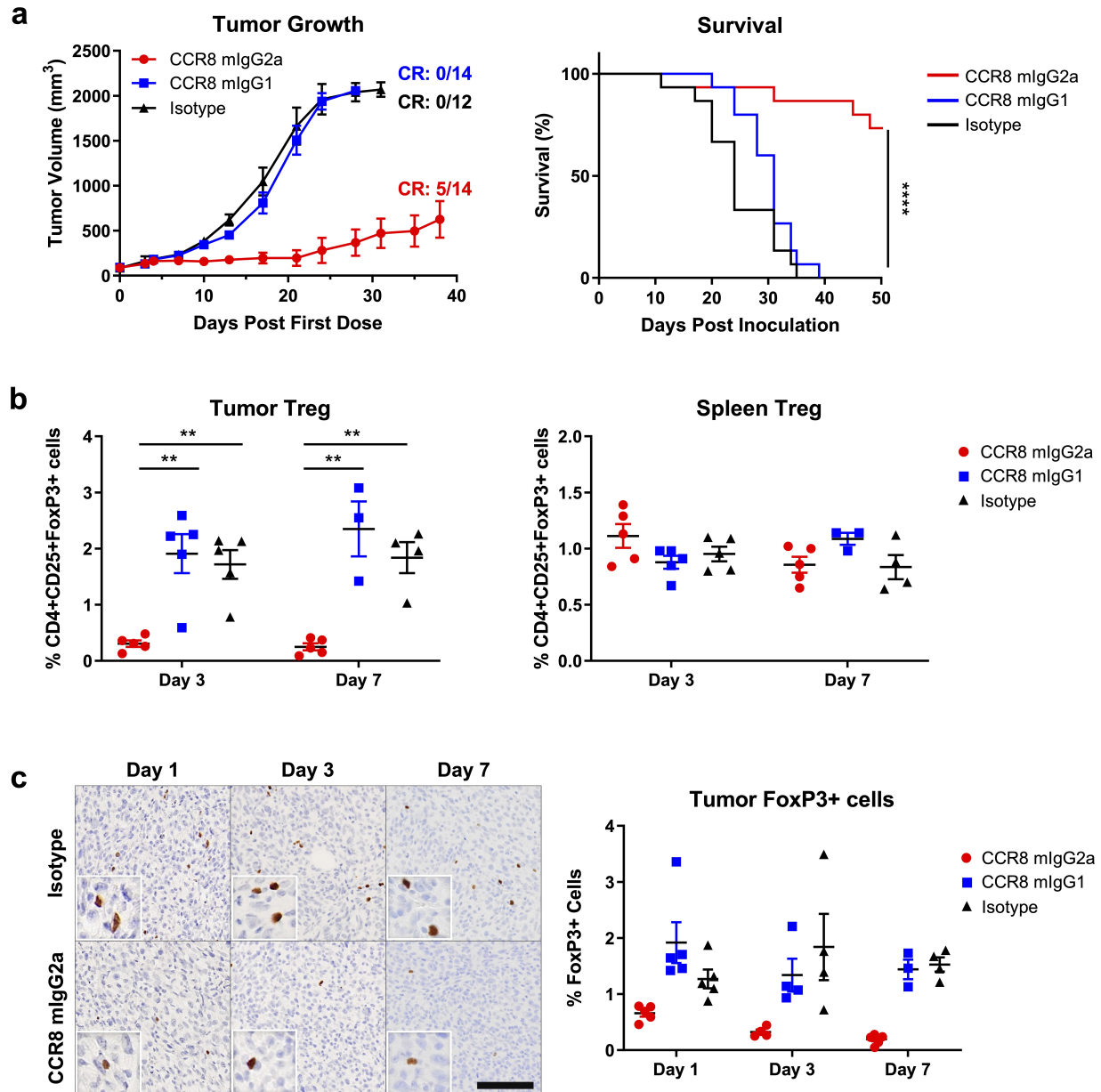


**Figure 3.** Depletion of CCR8<sup>+</sup> tumor Tregs is required for antitumor efficacy of anti-mouse CCR8 Ab in the MC38 model.

a) Tumor growth (left) and survival (right) analysis of cohorts of C57BL/6 mice bearing MC38 tumors and treated with the indicated antibodies. Mice were randomized into treatment groups when average tumor volume was approximately 100mm<sup>3</sup>. Day0 indicates day of first dose (left) or tumor inoculation (right). Tumor growth curves show average  $\pm$  SEM; CR corresponds to the number of complete responses in each group. Survival p values were obtained with a pairwise Log-rank (Mantel-Cox) test (\*\*\*\*:  $p < 0.0001$ ). b) Flow cytometry analysis on tumor immune infiltrate and spleens from MC38 tumor-bearing mice treated with either one (Day 3) or two (Day 7) doses of the indicated antibodies. Days refer to time after first dose. Graphs show the percentages of Tregs (CD4+CD25+FoxP3+) out of live CD45+CD3+ cells in the tumor (right) and spleen (left). c) IHC analysis of FoxP3+ cells in MC38 tumors from mice treated with the indicated antibodies as in (b). Representative images are shown on the left and summary graphs on the right. In (b) and (c) data is presented as average  $\pm$  SEM. ANOVA was used to compare the three treatment arms, followed by Tukey's multiple comparison post hoc test to evaluate differences between the individual treatment arms. p values are shown for statistically significant differences (\*:  $p = 0.01$  to  $0.05$ ; \*\*:  $p = 0.001$  to  $0.01$ ; \*\*\*\*:  $p < 0.001$ ).

tumor Tregs was detectable from day 1 after administration of a single dose of anti-mouse CCR8 mIgG2a (Figure 3c) and was sustained up to day 7 (Figures 3b and 3c). Moreover, this effect was specific for tumor Tregs, as no depletion was detected in splenic Tregs (Figure 3b, right panel) or in other T cell subsets (Figure 4a and Supplementary Figure 5c), where CCR8 expression is low (Supplementary Figure 3). Depletion of CCR8-positive Tregs could trigger compensatory changes in remaining Tregs or in non-Treg CD4 T cells subsets, resulting in a more immunosuppressive phenotype. We therefore verified that FoxP3 expression was not affected in tumor CD4 T cells upon treatment with anti-mouse CCR8 mIgG2a Ab (Supplementary Figure 5b). Gene expression analysis also showed no increase in expression of genes associated with suppressive Treg function, such as TIGIT, CTLA-4 and ICOS, in MC38 tumors from mice treated with either anti-mouse CCR8 mIgG2a or mIgG1 antibody (Supplementary Figure 6).

### **Anti-mouse CCR8 mIgG2a Ab treatment induces CD8 infiltration, proinflammatory responses, and immunological memory**

We further characterized immune cell infiltration in MC38 tumors upon anti-mouse CCR8 Ab treatment by flow cytometry. In a subset of the tumors that showed decreased Treg infiltration (Figure 3b) we detected a concomitant increase in CD8 infiltration, which resulted in increased CD8-to-FoxP3 ratios (Figure 4a). No changes were observed in other immune cell populations, including Tconv, CD19 + B cells, or CD11b+ myeloid cells (Supplementary Figure 5c). Percentage of tumor CD8 T cells increased over time and IHC analysis demonstrated robust infiltration throughout the tumor tissue (Figure 4b). To more broadly assess changes in the tumor microenvironment, we then performed gene expression analysis in MC38 tumors after one dose of anti-mouse CCR8 mIgG2a or mIgG1 using a NanoString mouse immunology panel. Samples from animals treated with anti-mouse CCR8 mIgG1 and isotype control clustered together and were more similar to each other than to anti-mouse CCR8 mIgG2a-treated samples using unsupervised clustering. No genes were significant in the differential gene expression analysis after correction for false discovery rate. However, genes with greater than one log fold-change in expression in anti-CCR8 mIgG2a-treated compared to anti-CCR8 mIgG1-treated and isotype-treated samples showed upregulation of chemokine ligands and interleukins involved in pro-inflammatory responses (Figure 4c). Additionally, gene set enrichment analysis (GSEA) of anti-CCR8 mIgG2a-treated compared to isotype-treated samples revealed upregulated genes are enriched in inflammatory, interferon- $\alpha$ , and interferon- $\gamma$  responses (Table 1). These data suggest that treatment with Fc-competent anti-mouse CCR8 Ab can efficiently deplete tumor Tregs, resulting in increased CD8 T cell activity and anti-tumor responses. As CD8 T cell activation is expected to lead to establishment of immunological memory, we performed tumor re-challenge studies to assess the durability of response to anti-CCR8 mIgG2a treatment. Mice whose MC38 tumors

had been previously eradicated by treatment with anti-mouse CCR8 mIgG2a Ab were re-implanted with MC38 and B16-F10 tumors on contralateral flanks. As a control, tumor-naïve and untreated age-matched mice were also challenged with MC38 and B16-F10 contralaterally. All naïve mice developed tumors on both flanks, with the exception of a single MC38 tumor that initially grew out and then regressed (Figure 4d). In the re-challenged mouse cohort, all mice remained MC38 tumor-free up to day 45 after tumor inoculation, with a single MC38 tumor growing by day 50. On the contrary, 8 out of ten re-challenged mice developed B16-F10 tumors (Figure 4d), albeit their growth appeared to be slower as compared to naïve mice, as previously reported for other therapeutic approaches (e.g.)<sup>33</sup>

### **The anti-human CCR8 antibody GS-1811 specifically binds to human CCR8 and inhibits CCR8 downstream signaling**

To discover anti-human CCR8 antibodies, we performed mouse immunizations and generated a panel of hybridomas that were selected for binding to CHO cells engineered to express human CCR8 but not to parental CHO cells or to CHO cells expressing the closely related CCR4 receptor (data not shown). The top candidate from this selection was then humanized to generate GS-1811, which was constructed with the human IgG1/kappa isotype backbone and expressed in a host cell line devoid of core fucosylation of N-linked glycans. As afucosylated hIgG1 shows higher Fc $\gamma$ R binding affinity and can outcompete endogenous IgG for binding to CD16 for enhanced ADCC,<sup>34</sup> GS-1811 is optimized to selectively deplete tumor-infiltrating Treg cells. Similarly to its parental Ab, GS-1811 is specific for human CCR8, as determined by binding to human CCR8-expressing and not CCR4-expressing CHO cells (Figure 5a) and is able to potently inhibit CCL1-induced signaling downstream of CCR8 (Figure 5b). On-cell affinity of GS-1811 was determined to be about 17pM (Figure 5c). We also confirmed that GS-1811 binds specifically to tumor-infiltrating Tregs isolated from human primary tumor samples, but only poorly to tumor Tconv or CD8 T cells, and to peripheral Treg or Tconv cells from healthy PBMCs (Figure 5d).

### **GS-1811 mediates ADCC of target cells expressing CCR8 at levels comparable to tumor-infiltrating Tregs**

GS-1811 does not bind to mouse or monkey CCR8 thus limiting our ability to directly verify its effect *in vivo*. Therefore, to test the ability of GS-1811 to specifically deplete human tumor-infiltrating Tregs, while sparing peripheral Tregs and other T cell subsets, we generated a panel of CHO cells lines expressing increasing densities of human CCR8, from 600 to over 10000 molecules per cell. We then assessed *in vitro* ADCC activity of GS-1811 and fucosylated (fuc) GS-1811 toward this CHO cell line panel in the presence of freshly isolated NK cells from healthy human donors. While fucosylated GS-1811 depleting activity was low for target cells expressing less than 5000 CCR8 molecules, afucosylated GS-1811 robustly depleted cells expressing 2500 CCR8 molecules (Figure 6a, 6b), which is within the range of CCR8 expression in human tumors (Figure 1c). Importantly, despite its enhanced ADCC potential, GS-1811 was not efficient at

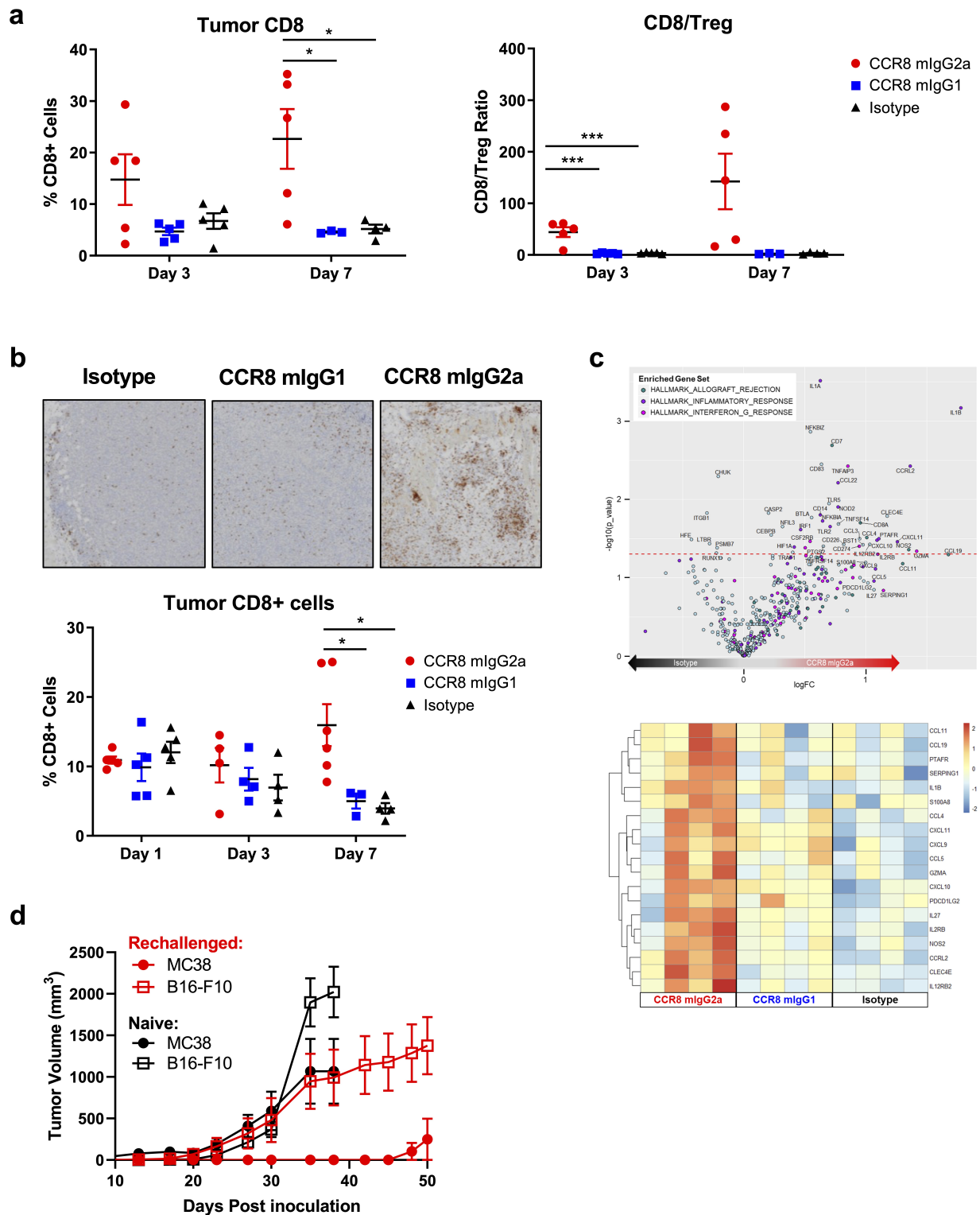


**Figure 4.** Depletion of CCR8+ tumor Tregs induces CD8 infiltration, proinflammatory responses and immunological memory.

a) Flow cytometry analysis on tumor immune infiltrate from MC38 tumor-bearing mice treated with either one (Day 3) or two (Day 7) doses of the indicated antibodies. Days refer to time after first dose. Graphs show the percentages of CD8+ T cells out of live CD45+CD3+ cells (right) and the ratio of CD8/Treg cells (left) in the tumors. b) IHC analysis of CD8+ cells in MC38 tumors from mice treated with the indicated antibodies as in (a). Representative images from the Day7 group are shown on top, summary graphs on the bottom. In (a) and (b) data is presented as average  $\pm$  SEM. ANOVA was used to compare the three treatment arms, followed by Tukey's multiple comparison post hoc test to evaluate differences between the individual treatment arms. p values are shown for statistically significant differences (\*:  $p=0.01$  to  $0.05$ ; \*\*:  $p=0.001$  to  $0.01$ ; \*\*\*:  $p<0.001$ ). c) NanoString gene expression analysis on MC38 tumors from mice treated with a single dose of anti-mouse CCR8 Ab in the mlgG2a or mlgG1 format or with isotype control;  $n=4$  per group, evaluated at day 3 after dosing. Top: volcano plot showing differential gene expression between anti-mouse CCR8 mlgG2a and isotype groups; bottom: genes with greater than one log fold-change in expression in anti-CCR8 mlgG2a compared to anti-CCR8 mlgG1 and isotype samples. d) Tumor growth upon rechallenge in MC38 tumor-bearing mice that were fully cured by anti-mouse CCR8 antibody treatment (red) or in naïve mice as control (black). Mice were inoculated with MC38 and B16-F10 tumor cells on contralateral flanks. Curves represent average  $\pm$  SEM.

depleting cells with CCR8 expression below 1500 molecules/cells (Figure 6a, Table 2), within the range of peripheral T cell subsets or tumor-infiltrating Tconv and CD8 T cells. To evaluate the effect of GS-1811-mediated ADCC on cells endogenously expressing CCR8 at densities within the range observed on tumor-infiltrating Tregs, we performed ADCC assays using the Hut78 cell line. The average EC50 across three NK cell donors was  $0.0017 \pm 0.0012$  and average maximum killing was  $67.5 \pm 2.69\%$  (Figure 6c). Finally, we assessed ADCC in TILs from different tumor types using exogenously added NK cells. Results from three tumor types

and two independent NK cell donors showed that percentages of Tregs were consistently reduced upon incubation with afucosylated GS-1811 as compared to isotype control (Figure 6d), indicating that GS-1811 can promote killing of tumor-infiltrating Tregs *ex vivo*.

## Discussion

It is well established that the presence of tumor Treg cells is associated with poor prognosis in cancer,<sup>4–6</sup> likely resulting from a more immunosuppressive TME.<sup>35–37</sup> In this case, strategies to reduce tumor Tregs by their destruction via natural killer (NK) cells and by inhibiting their trafficking into the tumor would be expected to result in a less suppressive TME,<sup>38,39</sup> leading to anti-tumor immunity. Therefore, in this study we present evidence that tumor Tregs selectively express CCR8 and that targeting CCR8 *in vivo* results in improved survival with selective tumor Treg depletion. These data highlight the therapeutic potential of targeting CCR8, and we further present data on the generation of a selective and specific anti-human CCR8 antibody for clinical evaluation.

Through evaluation of TCGA and available single cell RNA sequence datasets, we found CCR8 expression to be highly

**Table 1.** Gene signatures significantly enriched in CCR8 mlgG2a-treated samples compared to isotype-treated samples.

Gene Signature	ES	NOM p-val	FDR q-val
HALLMARK_ALLOGRAFT_REJECTION	0.573035	0	0.053705
HALLMARK_INTERFERON_GAMMA_RESPONSE	0.538323	0.002	0.098711
HALLMARK_INFLAMMATORY_RESPONSE	0.528647	0.005	0.099991
HALLMARK_TNFA_SIGNALING_VIA_NFKB	0.518547	0.018	0.128644
HALLMARK_INTERFERON_ALPHA_RESPONSE	0.531989	0.109631	0.189229
HALLMARK_KRAS_SIGNALING_UP	0.510397	0.074975	0.162116

ES: enrichment score; NOM p-val: nominal p value; FDR q-val: false discovery rate-corrected q values. FDR q-val < 0.25 are considered significant.

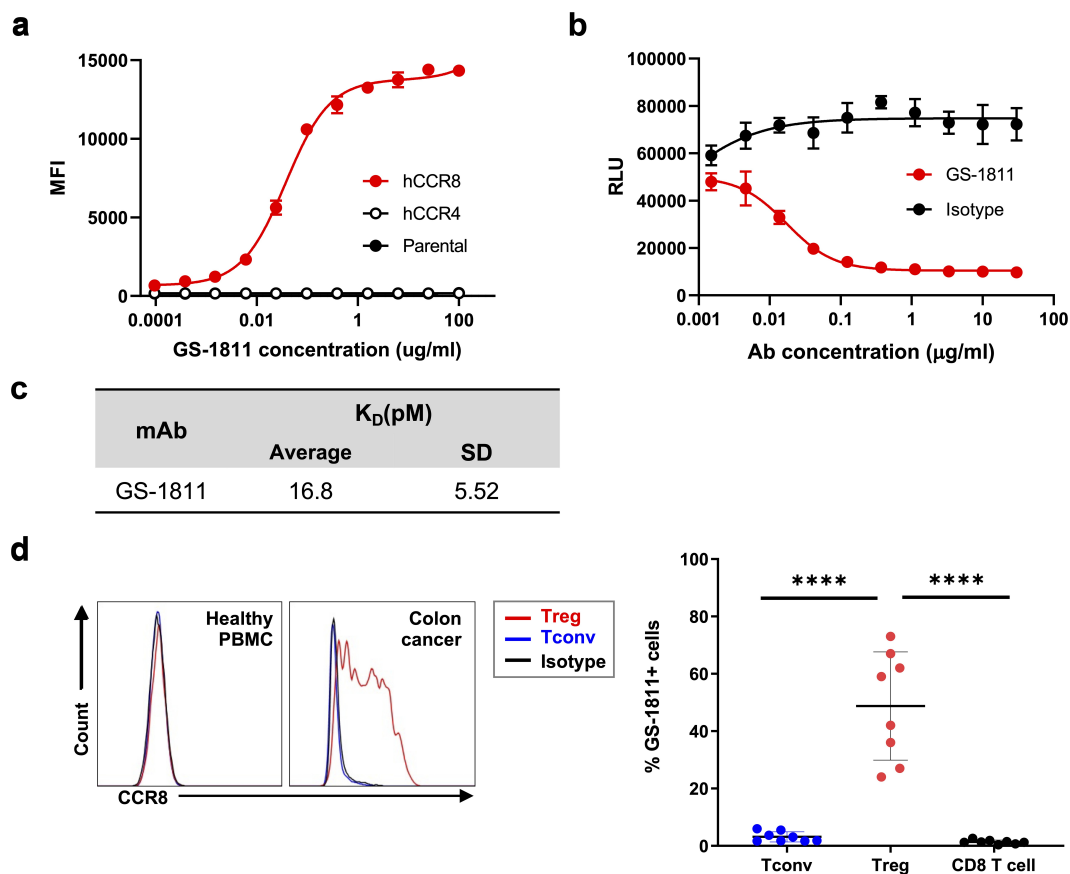


**Figure 5.** Human anti-CCR8 mAb GS-1811 binds specifically to human CCR8 and antagonizes its activity.

a) Specific binding of GS-1811 to CHO-S cells expressing hCCR8, hCCR4 or to control parental cell line as determined by flow cytometry. Each data point represents average of three replicates  $\pm$  SD. b) Antagonistic activity of GS-1811 in the presence of human CCL-1, evaluated by the PathHunter eXpress human CCR8 CHO-K1  $\beta$ Arrestin GPCR Assay. Each data point represents average of three replicates  $\pm$  SD. c) Summary of GS-1811 on-cell affinity as measured by MSD assay. Mean dissociation constant (KD) and standard deviation (SD) were calculated from 3 independent experiments. d) Flow cytometry analysis showing GS-1811 binding to different T cell populations from healthy PBMCs or human primary colon tumor samples; left: representative histograms; right: percentage of CCR8+ cells in Tconv (blue), Treg (red) and CD8 T cells (black) in 8 tumor samples. T cell subsets were identified as in Figure 1. Error bars represent standard deviation from the average. The degree of statistical significance between populations indicated on top of the graph (\*\*\*\*:  $p < 0.0001$ ).

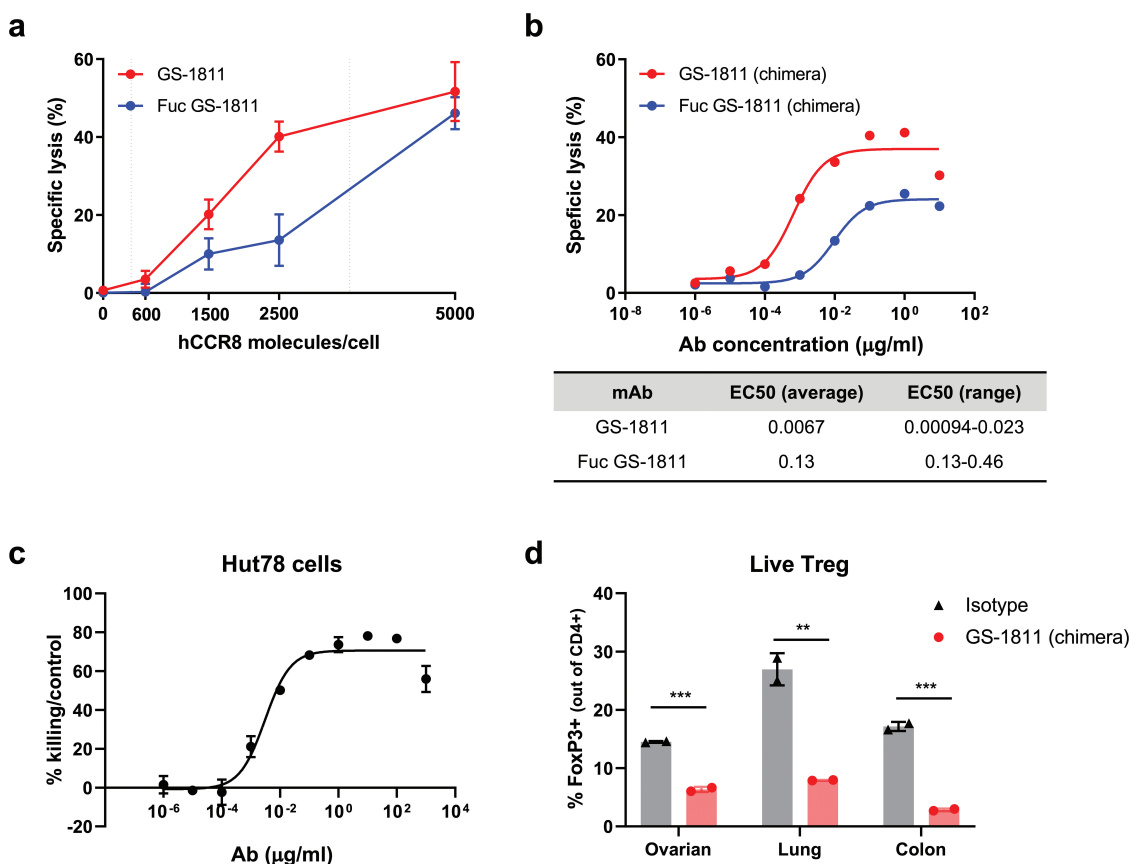


**Figure 6.** GS-1811 specifically mediates depletion of cells expressing CCR8 at densities comparable to tumor-infiltrating Tregs.

a) *In vitro* ADCC assay with a fixed concentration (1 µg/mL) of afucosylated or fucosylated (Fuc) versions of GS-1811 mAb against CHO cell lines expressing increasing densities of human CCR8 in presence of freshly isolated NK cells from healthy human donors (NK : target cell ratio, 5 : 1). Data is from one representative NK donor; error bars represent SD from technical triplicates. The dotted vertical lines represent average CCR8 densities in normal peripheral and tumor Tregs. b) ADCC activity measured against target cells expressing 2,500 CCR8 molecules/cell, with increasing concentrations of afucosylated or fucosylated (Fuc) chimeric version of GS-1811. One representative NK donor is shown in the graph. EC50 values (in µg/mL) from 10 independent donors are reported in the table on the bottom. c) GS-1811 ADCC activity on Hut78 cells endogenously expressing human CCR8. The curve is from one representative NK donor; error bars represent SD from technical triplicates. d) GS-1811 ADCC activity on TILs from primary human tumor samples in the presence of added NK cells from healthy donors. Tregs were identified as CD4+FoxP3+ out of live CD45+CD3+ cells. Data from one representative NK cell donor; error bars represent SD from technical duplicates.

**Table 2.** EC50 and maximum killing for GS-1811-mediated ADCC on CHO cells expressing increasing number of CCR8 molecules per cell.

CHO cell lines	Parental	hCCR8-600	hCCR8-1.5k	hCCR8-2.5k	hCCR8- 5k	hCCR8-10k
EC50 (ng/ml)	NA	NA	19 ± 0.24	6.9 ± 5.5	1.7 ± 1.6	3.0 ± 2.4
Max killing (%)	NA	NA	12 ± 6.22	17.63 ± 7.67	36.2 ± 13.06	27.7 ± 7.21

Average ± SD from two independent NK cell donors.

restricted to FoxP3+ tumor-infiltrating Tregs, consistent with previous reports.<sup>40,41</sup> Expression of CCR8 on tumor Tregs is more selective than other well-known Treg markers, including CD25, CTLA-4, GITR, TIGIT, and CCR4. CCR8 expression is higher in primary tumors than in normal adjacent tissues and significantly higher than in peripheral Tregs and both tumor and peripheral CD4+ T conventional cells. We also show that, on a per-cell basis, tumor Tregs have the highest number of CCR8 molecules compared to any other T cell subsets. CCR8+ Tregs are also known to be highly immunosuppressive.<sup>12,42</sup> Thus, taken together, these data establish CCR8 as a definitive and highly restricted immunosuppressive marker for tumor Tregs. Importantly, this suggests CCR8 may be a good therapeutic target for selective depletion of these cells.

Of note, previous reports have detailed CCR8 expression outside of the tumor and, most notably, in skin.<sup>18,19,43</sup> Here we demonstrate that, while both CCR8 and CCR4 are expressed on all skin T cell subsets, the absolute number of Tregs and CD8 T cells in the skin is very low (<1%). Therefore, we would not expect significant systemic effects upon treatment with a CCR8-depleting Ab above the relatively mild and reversible effects reported with CCR4-depleting Ab mogamulizumab in clinical settings.<sup>44</sup> This conclusion is also supported by the lack of treatment-related toxicities observed in our mouse studies.

In this study, we sought to evaluate the therapeutic impact of depletion of CCR8+ tumor Tregs in cancer using syngeneic mouse tumor models, where genetic deletion of FoxP3-expressing cells has been shown to inhibit tumor growth.<sup>45</sup>

We observed robust anti-tumor response upon treatment with an anti-mouse CCR8 Ab in a variety of mouse tumor models, and efficacy was maintained also when treating larger tumors. In the MC38 model, anti-tumor response was dependent on the ability of the anti-mouse CCR8 Ab to engage with Fc receptors<sup>32</sup> and mediate efficient Treg depletion. Importantly, depletion was specific to tumor Tregs, and not detected in splenic Tregs or other T cell subsets. While we cannot exclude that CCR8 could be expressed transiently and/or on a small percentage of non-Treg cells, possibly leading to their depletion, our observation that lower levels of CCR8 lead to reduced potential for ADCC suggests that achieving a therapeutic window for effective and selective depletion of tumor-infiltrating Tregs could be feasible in clinical settings.

In MC38 tumors, decrease in tumor-infiltrating Tregs was associated with an increase in CD8 infiltration, which resulted in increased CD8-to-FoxP3 ratio. Importantly, the increased CD8-to-FoxP3 ratio suggests that, concomitant with a loss of tumor Treg cells, there is a shift in immunological profile favoring an anti-tumor response, which is consistent with favorable prognosis in human cancer.<sup>1,46,47</sup> In fact, gene expression analyses revealed a shift toward upregulation of chemokine ligands and interleukins involved in pro-inflammatory responses associated with the tumor Treg cell loss seen upon treatment with the mIgG2a anti-CCR8 Ab. This was corroborated by GSEA, which revealed upregulated gene enrichment in inflammatory, interferon- $\alpha$ , and interferon- $\gamma$  responses and further supports the notion that depleting tumor Tregs results in creation of a favorable anti-tumor immunological environment. In line with this hypothesis, as CD8 T cell activation is expected to lead to establishment of immunological memory,<sup>48</sup> we also demonstrated that mice whose MC38 tumors were previously eradicated by anti-mouse CCR8 mIgG2a Ab treatment were resistant to tumor re-challenge.

Tregs are highly malleable and can modulate their phenotype in response to extracellular signals in the tumor microenvironment.<sup>3,35</sup> We considered the possibility that depletion of CCR8-positive cells could promote a more suppressive phenotype in remaining Tregs, or that CCR8 Ab treatment could otherwise affect Treg conversion,<sup>21</sup> but did not detect changes consistent with these hypotheses in our studies. Moreover, the increased CD8 T cell infiltration in the tumor, increased expression of pro-inflammatory markers, and significant anti-tumor efficacy observed upon anti-mouse CCR8 mIgG2a Ab treatment, all suggest remaining Tregs are not highly suppressive *in vivo*.

While we could not directly assess anti-tumor response in the immunophenotyping studies due to the shorter duration of treatment, it is tempting to speculate that the subset of mice showing robust CD8 T cell infiltration upon anti-CCR8 Ab treatment are the ones that are developing robust anti-tumor immunity, which would eventually result in complete response. We therefore hypothesized that relieving tumor T cell inhibition through PD-1 blockade could synergize with CCR8+ Treg depletion and selected the PD-1 resistant MBT-2 tumor model to test this hypothesis. Of note, MBT-2 tumors

are known to harbor a significantly greater proportion of CD4 + cells, compared with the PD-1 responsive MC38 model,<sup>49</sup> suggesting a greater degree of Treg infiltration as an underlying mechanism for PD-1 resistance. Indeed, we observed significantly increased anti-tumor efficacy with combination therapy as compared with either anti-PD-1 or anti-CCR8 monotherapy, clearly indicating that an anti-CCR8 Ab that depletes tumor Treg cells can synergize with established immunology therapeutic modalities to unleash robust anti-tumor responses.<sup>50</sup>

Given the highly restricted expression of CCR8 to tumor Tregs, and the robust *in vivo* data, we sought to identify anti-human CCR8 antibodies for clinical use. Through a hybridoma screen, we identified a top candidate, GS-1811. GS-1811 is specific for human CCR8 and selectively binds to tumor Treg but not to tumor T conventional or CD8 T cells, nor to peripheral Treg or Tconv cells. ADCC has been shown to depend on target density and on the Ab ability to engage FcRs.<sup>51</sup> Since a reduction in core fucosylation in the CH2 domain of the IgG1 Fc region has been shown to enhance ADCC function of an antibody via improved Fc $\gamma$ RIIIA binding,<sup>30</sup> we expressed GS-1811 in cell line devoid of N-linked glycan core fucosylation, which leads to an afucosylated IgG1 backbone. Using a carefully validated panel of target cells expressing increasing number of CCR8 molecules per cell combined with our precise quantification of CCR8 expression on a per-cell basis in tumor and peripheral T cell subsets, we were able to establish that the afucosylated GS-1811, but not a fucosylated version, efficiently depletes cells in which the density of receptor expression is greater than 2500 CCR8 molecules per cell, which is within the physiological level detected on human tumor Treg cells. Importantly, GS-1811 has low depleting activity toward cells expressing CCR8 within the range of peripheral T cell subsets or tumor-infiltrating Tconv and CD8 T cells. These data suggest that cells expressing CCR8 at levels similar to peripheral Tregs will not be subject to Fc-mediated ADCC by GS-1811 while cells expressing CCR8 at levels similar to tumor Tregs will be depleted via Fc-mediated ADCC in the presence of GS-1811. It should be noted that GS-1811 also potently inhibits CCL-1-induced signaling downstream of CCR8. While we believe that ADCC-mediated Treg depletion is the key mechanism of action of GS-1811, blockade of CCR8 function might also impact Treg cell survival and/or conversion, as demonstrated in mouse studies,<sup>21,52</sup> contributing to decreased Treg function and anti-tumor effects. Overall, our data support ongoing clinical development of GS-1811 (NCT05007782) to target CCR8 in cancer in order to drive tumor Treg depletion and to shift the immunological milieu toward promoting anti-tumor immunity.

## Acknowledgments

We are grateful to all Jounce Therapeutics and Gilead Sciences employees that contributed to the GS-1811 project and whose work could not be included in this manuscript. We thank Dr. James Allison for providing the MC38 cell line and the CHTN and NDRI for providing tissue specimens. Jounce Therapeutics dedicates this manuscript to the memory of our colleague and co-author of this study Edward C. Stack, Ph.D.

## Disclosure statement

JAB, MW, TR, AM, VS, MP, SJ, AS, KK, YE, MAM, DW and MG are employees and own stock of Jounce Therapeutics. JDW, ECS, FD, BK, CF, RK, LM, KL, CX, YZ, CH, DU, CX, YZ and DRS were Jounce Therapeutics employees at the time of the study. DSA, MRK and BMW are employees and own stock of Gilead Sciences.

## Funding

The author(s) reported there is no funding associated with the work featured in this article.

## Data availability statement

The single-cell RNA-sequencing data that support the findings in Figure 1b are openly available in Gene Expression Omnibus at <https://www.ncbi.nlm.nih.gov/geo/>, reference numbers GSE72056, GSE103322, GSE98638. The RNA-seq gene expression data of CCR8 referenced in Figure 1c from QIAGEN OmicSoft OncoLand database TCGA\_B38\_GC33\_20210915\_v2 were used under license for this study. Data are available from the authors upon request with permission from QIAGEN Digital Insights. The mouse gene expression data referenced in Figure 4c are available from the authors upon reasonable request.

## References

- Lee HM, Bautista JL, Hsieh CS. Thymic and peripheral differentiation of regulatory T cells. *Adv Immunol.* 2011;112:25–71.
- Josefowicz SZ, Lu LF, Rudensky AY. Regulatory T cells: mechanisms of differentiation and function. *Annu Rev Immunol.* 2012;30:531–564. doi:10.1146/annurev.immunol.25.022106.141623.
- Gasner A, Plitas G. Tumor resident regulatory T cells. *Semin Immunol.* 2021;52:101476. doi:10.1016/j.smim.2021.101476.
- Fu J, Xu D, Liu Z, Shi M, Zhao P, Fu B, Zhang Z, Yang H, Zhang H, Zhou C, et al. Increased regulatory T cells correlate with CD8 T-cell impairment and poor survival in hepatocellular carcinoma patients. *Gastroenterology.* 2007;132:2328–2339. doi:10.1053/j.gastro.2007.03.102.
- Petersen RP, Campa MJ, Sperlazza J, Conlon D, Joshi MB, Harpole DH Jr., Patz EF Jr. Tumor infiltrating Foxp3+ regulatory T-cells are associated with recurrence in pathologic stage I NSCLC patients. *Cancer.* 2006;107:2866–2872. doi:10.1002/cncr.22282.
- Shen Z, Zhou S, Wang Y, Li RL, Zhong C, Liang C, Sun Y. Higher intratumoral infiltrated Foxp3+ Treg numbers and Foxp3+/CD8+ ratio are associated with adverse prognosis in resectable gastric cancer. *J Cancer Res Clin Oncol.* 2010;136:1585–1595. doi:10.1007/s00432-010-0816-9.
- Kamada T, Togashi Y, Tay C, Ha D, Sasaki A, Nakamura Y, Sato E, Fukuoka S, Tada Y, Tanaka A, et al. PD-1(+) regulatory T cells amplified by PD-1 blockade promote hyperprogression of cancer. *Proc Natl Acad Sci U S A.* 2019;116:9999–10008. doi:10.1073/pnas.1822001116.
- Saleh R, Elkord E. Treg-mediated acquired resistance to immune checkpoint inhibitors. *Cancer Lett.* 2019;457:168–179. doi:10.1016/j.canlet.2019.05.003.
- Kumagai S, Togashi Y, Kamada T, Sugiyama E, Nishinakamura H, Takeuchi Y, Vitaly K, Itahashi K, Maeda Y, Matsui S, et al. The PD-1 expression balance between effector and regulatory T cells predicts the clinical efficacy of PD-1 blockade therapies. *Nat Immunol.* 2020;21:1346–1358. doi:10.1038/s41590-020-0769-3.
- Tan CL, Kuchroo JR, Sage PT, Liang D, Francisco LM, Buck J, Thaker YR, Zhang Q, McArdel SL, Juneja VR, et al. PD-1 restraint of regulatory T cell suppressive activity is critical for immune tolerance. *J Exp Med.* 2021;218. doi:10.1084/jem.20182232
- Andrew DP, Ruffing N, Kim CH, Miao W, Heath H, Li Y, Murphy K, Campbell JJ, Butcher EC, Wu L. C-C chemokine receptor 4 expression defines a major subset of circulating nonintestinal memory T cells of both Th1 and Th2 potential. *J Immunol.* 2001;166(1):103–111. doi:10.4049/jimmunol.166.1.103.
- Plitas G, Konopacki C, Wu K, Bos PD, Morrow M, Putintseva EV, Chudakov DM, Rudensky AY. Regulatory T cells exhibit distinct features in human breast cancer. *Immunity.* 2016;45:1122–1134. doi:10.1016/j.immuni.2016.10.032.
- Bhatt D, Kang B, Sawant D, Zheng L, Perez K, Huang Z, Sekirov L, Wolak D, Huang JY, Liu X, et al. STARTRAC analyses of scRNAseq data from tumor models reveal T cell dynamics and therapeutic targets. *J Exp Med.* 2021;218. doi:10.1084/jem.20201329
- Van Damme H, Dombrecht B, Kiss M, Roose H, Allen E, Van Overmeire E, Kancheva D, Martens L, Murgaski A, Bardet PMR, et al. Therapeutic depletion of CCR8(+) tumor-infiltrating regulatory T cells elicits antitumor immunity and synergizes with anti-PD-1 therapy. *J Immunother. Cancer.* 2021;9. doi:10.1097/CJI.0000000000000345.
- Knipfer L, Schulz-Kuhnt A, Kindermann M, Greif V, Symowski C, Voehringer D, Neurath MF, Atreya I, Wirtz S. A CCL1/CCR8-dependent feed-forward mechanism drives ILC2 functions in type 2-mediated inflammation. *J Exp Med.* 2019;216:2763–2777. doi:10.1084/jem.20182111.
- McCully ML, Ladell K, Andrews R, Jones RE, Miners KL, Roger L, Baird DM, Cameron MJ, Jessop ZM, Whitaker IS, et al. CCR8 expression defines tissue-resident memory T cells in human skin. *J Immunol.* 2018;200:1639–1650. doi:10.4049/jimmunol.1701377.
- Connolly S, Skrinjar M, Rosendahl A. Orally bioavailable allosteric CCR8 antagonists inhibit dendritic cell, T cell and eosinophil migration. *Biochem Pharmacol.* 2012;83:778–787. doi:10.1016/j.bcp.2011.12.021.
- Schaerli P, Ebert L, Willmann K, Blaser A, Roos RS, Loetscher P, Moser B. A skin-selective homing mechanism for human immune surveillance T cells. *J Exp Med.* 2004;199:1265–1275. doi:10.1084/jem.20032177.
- Barshesht Y, Wildbaum G, Levy E, Vitenshtein A, Akinseye C, Griggs J, Lira SA, Karin N. cells as master drivers of immune regulation. *Proc Natl Acad Sci U S A.* 2017;114:6086–6091. doi:10.1073/pnas.1621280114.
- Das S, Sarrou E, Podgrabinska S, Cassella M, Mungamuri SK, Feirt N, Gordon R, Nagi CS, Wang Y, Entenberg D, et al. Tumor cell entry into the lymph node is controlled by CCL1 chemokine expressed by lymph node lymphatic sinuses. *J Exp Med.* 2013;210:1509–1528. doi:10.1084/jem.20111627.
- Villarreal DO, L'Huillier A, Armington S, Mottershead C, Filippova EV, Coder BD, Petit RG, Princiotta MF. Targeting CCR8 induces protective antitumor immunity and enhances vaccine-induced responses in colon cancer. *Cancer Res.* 2018;78:5340–5348. doi:10.1158/0008-5472.CAN-18-1119.
- Hanson A, Elpek K, Duong E, Shallberg L, Fan M, Johnson C, Wallace M, Mabry GR, Sazinsky S, Pepper L, et al. ICOS agonism by JTX-2011 (vopratelimab) requires initial T cell priming and Fc cross-linking for optimal T cell activation and anti-tumor immunity in preclinical models. *PLoS One.* 2020;15:e0239595. doi:10.1371/journal.pone.0239595.
- Blair T, Baird J, Bambina S, Kramer G, Gostissa M, Harvey CJ, Gough MJ, Crittenden MR. ICOS is upregulated on T cells following radiation and agonism combined with radiation results in enhanced tumor control. *Sci Rep.* 2022;12:14954. doi:10.1038/s41598-022-19256-8.
- Mootha VK, Lepage P, Miller K, Bunkenborg J, Reich M, Hjerrild M, Delmonte T, Villeneuve A, Sladek R, Xu F, et al. Identification of a gene causing human cytochrome c oxidase deficiency by integrative genomics. *Proc Natl Acad Sci U S A.* 2003;100:605–610. doi:10.1073/pnas.242716699.
- Subramanian A, Tamayo P, Mootha VK, Mukherjee S, Ebert BL, Gillette MA, Paulovich A, Pomeroy SL, Golub TR, Lander ES, et al. Gene set enrichment analysis: a knowledge-based approach for

- interpreting genome-wide expression profiles. *Proc Natl Acad Sci U S A.* 2005;102:15545–15550. doi:10.1073/pnas.0506580102.
26. Puram SV, Tirosh I, Parkh AS, Patel AP, Yizhak K, Gillespie S, Rodman C, Luo CL, Mroz EA, Emerick KS, et al. Single-cell transcriptomic analysis of primary and metastatic tumor ecosystems in head and neck cancer. *Cell.* 2017;171:1611–1624 e1624. doi:10.1016/j.cell.2017.10.044.
  27. Tirosh I, Izar B, Prakadan SM, Wadsworth MH 2nd, Treacy D, Trombetta JJ, Rotem A, Rodman C, Lian C, Murphy G, et al. Dissecting the multicellular ecosystem of metastatic melanoma by single-cell RNA-seq. *Science.* 2016;352:189–196. doi:10.1126/science.aad0501.
  28. Zheng C, Zheng L, Yoo JK, Guo H, Zhang Y, Guo X, Kang B, Hu R, Huang JY, Zhang Q, et al. Landscape of infiltrating T cells in liver cancer revealed by single-cell sequencing. *Cell.* 2017;169:1342–1356 e1316. doi:10.1016/j.cell.2017.05.035.
  29. Eisenberg E, Levanon EY. Human housekeeping genes, revisited. *Trends Genet.* 2013;29:569–574. doi:10.1016/j.tig.2013.05.010.
  30. Yamane-Ohnuki N, Satoh M. Production of therapeutic antibodies with controlled fucosylation. *MAbs.* 2009;1:230–236. doi:10.4161/mabs.1.3.8328.
  31. Colantonio L, Iellem A, Sinigaglia F, D'Ambrosio D. Skin-homing CLA+ T cells and regulatory CD25+ T cells represent major subsets of human peripheral blood memory T cells migrating in response to CCL1/I-309. *Eur J Immunol.* 2002;32:3506–3514.
  32. Nimmerjahn F, Ravetch JV. Divergent immunoglobulin g subclass activity through selective Fc receptor binding. *Science.* 2005;310:1510–1512. doi:10.1126/science.1118948.
  33. Nakamura K, Karmokar A, Farrington PM, James NH, Ramos-Montoya A, Bickerton SJ, Hughes GD, Illidge TM, Cadogan EB, Davies BR, et al. Inhibition of DNA-PK with AZD7648 sensitizes tumor cells to radiotherapy and induces type I IFN-dependent durable tumor control. *Clin Cancer Res.* 2021;27:4353–4366. doi:10.1158/1078-0432.CCR-20-3701.
  34. Iida S, Misaka H, Inoue M, Shibata M, Nakano R, Yamane-Ohnuki N, Wakitani M, Yano K, Shitara K, Satoh M. Nonfucosylated therapeutic IgG1 antibody can evade the inhibitory effect of serum immunoglobulin G on antibody-dependent cellular cytotoxicity through its high binding to FcγRIIIa. *Clin Cancer Res.* 2006;12:2879–2887. doi:10.1158/1078-0432.CCR-05-2619.
  35. Hatzioannou A, Boumpas A, Papadopoulou M, Papafragkos I, Varveri A, Alissafi T, Verginis P. Regulatory T cells in autoimmunity and cancer: a duplicitous Lifestyle. *Front Immunol.* 2021;12:731947. doi:10.3389/fimmu.2021.731947.
  36. Roychoudhuri R, Eil RL, Restifo NP. The interplay of effector and regulatory T cells in cancer. *Curr Opin Immunol.* 2015;33:101–111. doi:10.1016/j.coi.2015.02.003.
  37. Scott EN, Gocher AM, Workman CJ, Vignali DAA. Regulatory T cells: barriers of immune infiltration into the tumor microenvironment. *Front Immunol.* 2021;12:702726. doi:10.3389/fimmu.2021.702726.
  38. Ohue Y, Nishikawa H. Regulatory T (Treg) cells in cancer: can Treg cells be a new therapeutic target? *Cancer Sci.* 2019;110:2080–2089. doi:10.1111/cas.14069.
  39. Whiteside TL. FOXP3+ Treg as a therapeutic target for promoting anti-tumor immunity. *Expert Opin Ther Targets.* 2018;22:353–363. doi:10.1080/14728222.2018.1451514.
  40. Campbell JR, McDonald BR, Mesko PB, Siemers NO, Singh PB, Selby M, Sproul TW, Korman AJ, Vlach LM, Houser J, et al. Fc-optimized Anti-CCR8 antibody depletes regulatory T cells in human tumor models. *Cancer Res.* 2021;81:2983–2994. doi:10.1158/0008-5472.CAN-20-3585.
  41. De Simone M, Arrigoni A, Rossetti G, Gruarin P, Ranzani V, Politano C, Bonnal RJP, Provasi E, Sarnicola ML, Panzeri I, et al. Transcriptional landscape of human tissue lymphocytes unveils uniqueness of tumor-infiltrating T regulatory cells. *Immunity.* 2016;45:1135–1147. doi:10.1016/j.immuni.2016.10.021.
  42. Whiteside SK, Grant FM, Gyori DS, Conti AG, Imianowski CJ, Kuo P, Nasrallah R, Sadiyah F, Lira SA, Tacke F, et al. CCR8 marks highly suppressive Treg cells within tumours but is dispensable for their accumulation and suppressive function. *Immunology.* 2021;163:512–520.
  43. Gombert M, Dieu-Nosjean MC, Winterberg F, Bunemann E, Kubitzka RC, Da Cunha L, Haahtela A, Lehtimäki S, Müller A, Rieker J, et al. CCL1-CCR8 interactions: an axis mediating the recruitment of T cells and Langerhans-type dendritic cells to sites of atopic skin inflammation. *J Immunol.* 2005;174:5082–5091. doi:10.4049/jimmunol.174.8.5082.
  44. Kurose K, Ohue Y, Wada H, Iida S, Ishida T, Kojima T, Doi T, Suzuki S, Isobe M, Funakoshi T, et al. Phase Ia study of FoxP3+ CD4 Treg depletion by infusion of a humanized Anti-CCR4 antibody, KW-0761, in cancer patients. *Clin Cancer Res.* 2015;21:4327–4336. doi:10.1158/1078-0432.CCR-15-0357.
  45. Teng MW, Ngiow SF, von Scheidt B, McLaughlin N, Sparwasser T, Smyth MJ. Conditional regulatory T-cell depletion releases adaptive immunity preventing carcinogenesis and suppressing established tumor growth. *Cancer Res.* 2010;70:7800–7809. doi:10.1158/0008-5472.CAN-10-1681.
  46. Feng TT, Zou T, Wang X, Zhao WF, Qin AL. Clinical significance of changes in the Th17/Treg ratio in autoimmune liver disease. *World J Gastroenterol.* 2017;23:3832–3838. doi:10.3748/wjg.v23.i21.3832.
  47. Tavares MC, Sampaio CD, Lima GE, Andrade VP, Gonçalves DG, Macedo MP, Cordeiro de Lima VC. A high CD8 to FOXP3 ratio in the tumor stroma and expression of PTEN in tumor cells are associated with improved survival in non-metastatic triple-negative breast carcinoma. *BMC Cancer.* 2021;21:901. doi:10.1186/s12885-021-08636-4.
  48. van Gisbergen K, Zens KD, Munz C. T-cell memory in tissues. *Eur J Immunol.* 2021;51:1310–1324. doi:10.1002/eji.202049062.
  49. Grasselly C, Denis M, Bourguignon A, Talhi N, Mathe D, Tourette A, Serre L, Jordheim LP, Matera EL, Dumontet C. The antitumor activity of combinations of cytotoxic chemotherapy and immune checkpoint inhibitors is model-dependent. *Front Immunol.* 2018;9:2100. doi:10.3389/fimmu.2018.02100.
  50. Aksoylar HI, Boussiotis VA. Treg cells: a foe in cancer immunotherapy? *Nat Immunol.* 2020;21:1311–1312. doi:10.1038/s41590-020-0801-7.
  51. Temming AR, de Taeye SW, de Graaf EL, de Neef LA, Dekkers G, Bruggeman CW, Koers J, Ligthart P, Nagelkerke SQ, Zimring JC, et al. Functional attributes of antibodies, effector cells, and target cells affecting NK cell-mediated antibody-dependent cellular cytotoxicity. *J Immunol.* 2019;203:3126–3135. doi:10.4049/jimmunol.1900985.
  52. Coghill JM, Fowler KA, West ML, Fulton LM, van Deventer H, McKinnon KP, Vincent BG, Lin K, Panoskaltzis-Mortari A, Cook DN, et al. CC chemokine receptor 8 potentiates donor Treg survival and is critical for the prevention of murine graft-versus-host disease. *Blood.* 2013;122:825–836. doi:10.1182/blood-2012-06-435735.